Preprint of ***Cox, G.M., Halverson, G.P., Denyszyn, S., Foden, J., Macdonald, F.A., 2018. Precambrian Research, 319, 144–157***.

Cryogenian magmatism along the north-western margin of Laurentia: Plume or Rift?

Grant M. Cox[1,2*], Galen P. Halverson[3], Steven Denyszyn[4], Francis A. Macdonald[4]

Abstract

Here we present a new U-Pb baddeleyite ID-TIMS age of 713.7 ± 0.9 Ma on the Tatonduk dykes, which occur as a mafic swarm near the Yukon-Alaska border in the Proterozoic Tatonduk inlier. The dykes are considered to be equivalent to the Pleasant Creek Volcanics, a stack of basaltic to intermediate flows that lie above a major erosional disconformity and immediately beneath iron formation-bearing Sturtian glacial deposits correlated with the early Cryogenian Rapitan Group. Hence, the Tatonduk dykes were emplaced during the Sturtian snowball Earth event and contribute to the growing body of geochronological data that indicate its onset ca. 717 Ma. Furthermore, this age provides direct evidence for the syn-glacial origin of Sturtian iron formation in the Tatonduk inlier. Considering their apparent overlap with what is inferred to represent the Franklin Large Igneous Province (LIP) of northern Canada, the Pleasant Creek Volcanics and Tatonduk dykes might logically be considered a far-flung component of the Franklin Large Igneous Province. However, they occur in an actively extending environment >1200 km from the plume head on Melville Island and do not obviously align with the Franklin dyke trend. Furthermore, major, trace and isotopic data on the Pleasant Creek Volcanics and Tatonduk dykes reveal a composition that is entirely unique from the Franklin LIP and most likely reflect melting of potassic- and trace element-enriched sub-continental lithospheric Mantle. These volcanics and dykes highlight the complexity in defining what constitutes a LIP. The Pleasant Creek Volcanics and Tatonduk dykes either represent a non-plume end-member composition of the Franklin LIP, or more likely, rift volcanics associated with extension along the actively extending margin of north-west Laurentia. Although the plume and rifting may be geodynamically linked, this interpretation suggests that this new age on the Tatonduk dykes does not constrain the timing of Franklin magmatism.

Keywords: Franklin Large Igneous Province, Cryogenian, Shoshonites, Snowball Earth, Rift Volcanics

Introduction

The record of mafic magmatism in northern Laurentia during the late Tonian to early Cryogenain (ca. 730–710 Ma) is dominated by magmatic events associated with the breakup of Rodinia and the emplacement of the Franklin Large Igneous Province (LIP) (Denyszyn et al., 2009b; Macdonald et al., 2010). LIP events are closely associated with continental breakup (Courtillot et al., 1999) and commonly involve the eruption of 10^5–10^6 km^3 of mafic magmas over a few million years or less (Sobolev et al., 2011). Where these eruptions take place on a continent, the result can be a massive Continental Flood Basalt (CFB) province that covers $>10^5$ km^2 with hundreds to thousands of metres of dominantly mafic lava flows.

Extrusive igneous rocks associated with the Franklin LIP in northern Canada are dominated by basalt to basaltic andesites (i.e., continental tholeiites; Bedard et al., 2016; Dostal et al., 1986), typical of most continental flood basalts (CFBs), and are thought to be derived from a deep-seated mantle plume (Dostal et al., 1986; Rainbird, 1993; Shellnutt et al., 2004).

However, no high temperature picrites have been reported. The Franklin LIP differs from many other examples of LIPs in that magmatism spanned >10 m.y. (based on currently ages; Fig. 1), and possibly as long as 15 m.y. if nearly coeval mafic magmatism in southwestern Siberia (Ernst et al., 2016) records an early phase of the event. The Franklin LIP was emplaced in tropical central Rodinia (Denyszyn et al., 2009b); Fig. 2) and the duration of its emplacement spanned the onset of early Cryogenian Sturtian glaciation (i.e., 717 Ma; Macdonald et al., 2010). It was also an exceptionally large event, with dykes extending > 1200 km from the hypothesized plume head centred on Melville Island (Fig. 2A). Ernst et al., (2008) estimated an original surface area of 2.2×10^6 km^2 for the Franklin LIP, but if Kikiktak basalts of the North Slope block of Arctic Alaska (Cox et al., 2015) and Siberian mafic intrusions also record the Franklin LIP, its original areal extent may have been much greater (Cox et al., 2016b).

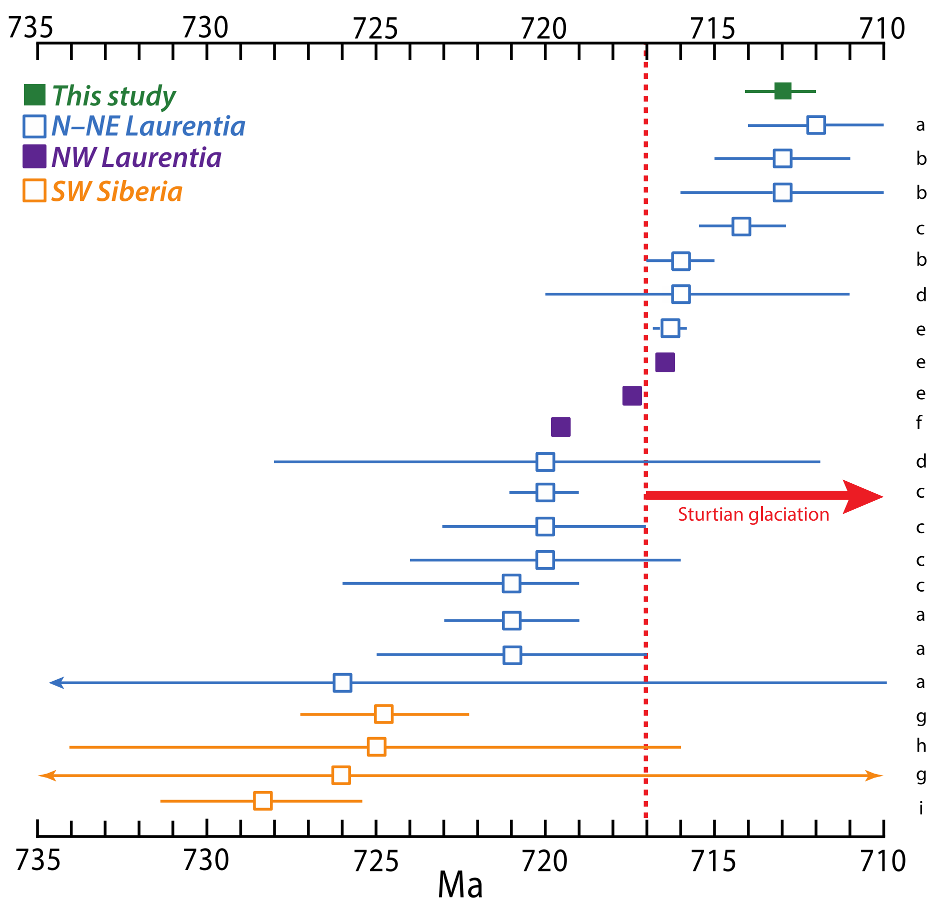

*Figure 1***.** *Temporal distribution of U-Pb zircon and baddeleyite ages on magmatic rocks in N-NE Laurentia broadly related to the Franklin Large Igneous Province (Denyszyn et al., 2009a), along with additional ages from NW Laurentia and Siberia that are tentatively ascribed to the Franklin event (Cox et al., 2016b; Ernst et al., 2016) . Sources radiometric ages:* ***a*** *(Denyszyn et al., 2009b) ,* ***b*** *(Denyszyn et al., 2009a),* ***c*** *(Heaman et al., 1992), recalculated from Macdonald and Wordsworth (2017),* ***d*** *(Pehrsson and Buchan, 1999),* ***e*** *(Macdonald et al., 2010),* ***f*** *(Cox et al., 2015),* ***g*** *(Ernst and Soderlund, 2012),* ***h,i*** *(Ariskin et al., 2013). Age of the onset of Sturtian glaciation from Macdonald et al. (2010).*

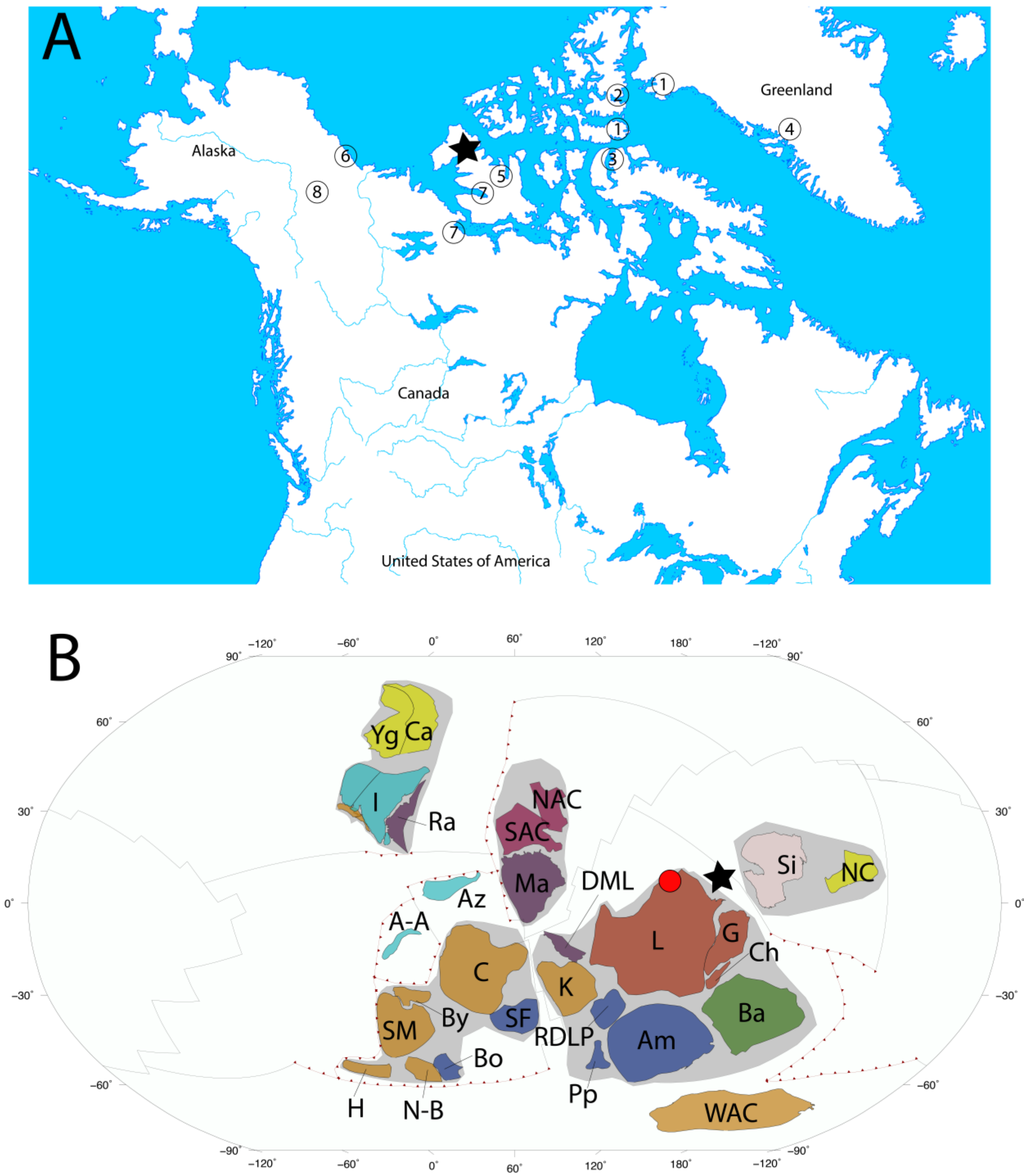

Figure 2. (A) Distribution of Franklin aged magmatism across Canada. Star denotes focal point of radial Franklin dykes - considered the approximate centre of the mantle plume source. (1) (Denyszyn et al., 2009a) (2) (Denyszyn et al., 2009b) (3) (Pehrsson and Buchan, 1999) (4) (Halls et al., 2010) (5) (Macdonald et al., 2010) (6) (Cox et al., 2015) (7) (Heaman et al., 1992) (8) this study. (B) Paleogeographic reconstruction from Merdith et. al., (2017) at ~ 750 Ma. A-A, Afif-Abas Terrane; Am, Amazonia; Az, Azania; Ba, Baltica; Bo, Borborema; By, Bayuda; Ca, Cathaysia (South China); C, Congo; Ch, Chortis; G, Greenland; H, Hoggar; I, India; K, Kalahari; L, Laurentia; Ma, Mawson; NAC, North Australian Craton; N-B, Nigeria-Benin; NC, North China; Pp, Paranapanema; Ra, Rayner (Antarctica); RDLP, Rio de la Plata; SAC, South Australian Craton; SF, São Francisco; Si, Siberia; SM, Sahara Metacraton; WAC, West African Craton. Shaded grey area is inferred extent of Rodinia and is meant as a guide only. Cratonic crust is coloured by present day geography: North America, red; South America, dark blue; Baltica, green; Siberia, grey; India and the Middle East, light blue; China, yellow; Africa, orange; Australia, crimson; Antarctica, purple.

The Pleasant Creek Volcanics and associated Tatonduk Dykes (hereafter referred jointly as the Tatonduk suite) of the Tatonduk inlier (Fig. 3) are a well-preserved mafic to andesitic suite that occurs stratigraphically below what are now recognized to be Sturtian–age glacial deposits and associated iron formation (Macdonald et al., 2009; Macdonald et al., 2010; Rooney et al., 2014; Strauss et al., 2013). Whereas previous unpublished K-Ar ages on these dykes yielded middle Ediacaran ages (Van Kooten et al., 1997), the occurrence of the Pleasant Creek Volcanics beneath Cryogenian strata and the fact that the dykes cross-cut Tonian strata indicate that both the lavas and dykes are equivalent and must be late Tonian to early Cryogenian in age (Macdonald et al., 2010; Macdonald et al., 2011). Importantly, because the volcanics rest above a major unconformity that truncates carbonates of the underlying Fifteenmile Group but appear to be transitional into the overlying Rapitan Group glacial deposits, we infer that the flows post-date onset of the Sturtian glaciation.

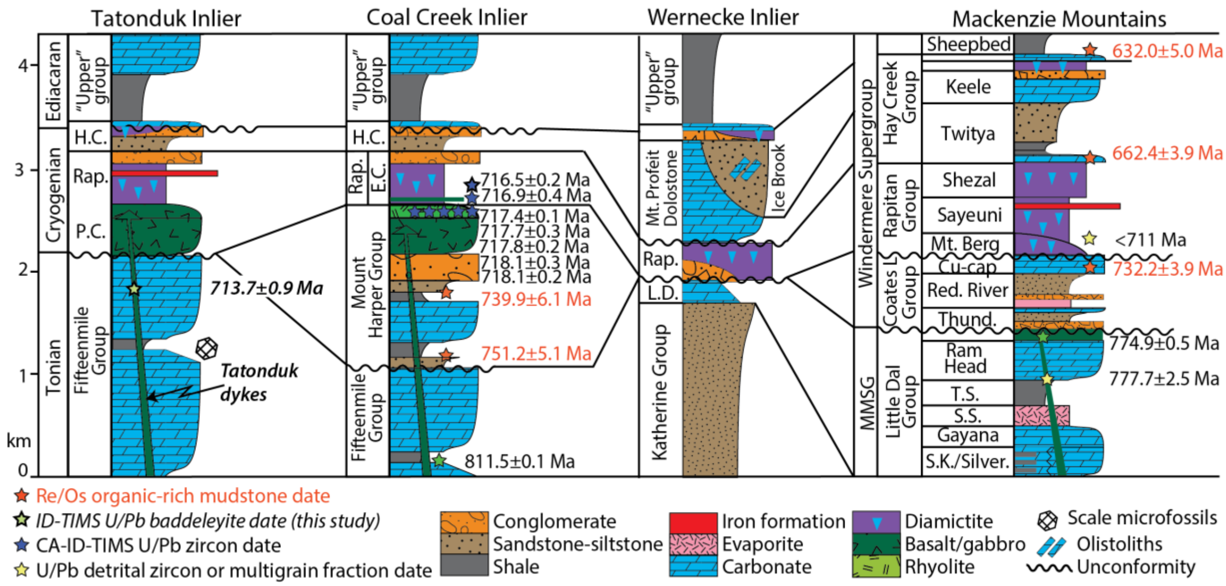

Figure 3. Schematic lithostratigraphic correlation middle Tonian to Ediacaran strata across four Proterozoic inliers spanning Yukon, modified from Macdonald et al. (in press) and references therein. H.C. = Hay Creek Group; Rap. = Rapitan; P.C. = Pleasant Creek Volcanics; E.C. = Eagle Creek Formation; L.D. = Little Dal Group; MMSG = Mackenzie Mountains Supergroup; Cu-cap = Copper Cap Formation; Thund. = Thundercloud Formation; S.K. = Stone Knife Formation; Silver. = Silverberry Formation T.S. = Ten Stone Formation; S.S. = Snail Spring Formation. Note that the thick Mount Harper Group, which records the late Tonian in the Coal Creek Inlier, is entirely absent in the Tatonduk inlier, where the basal Cryogenian unconformity places the Pleasant Creek Volcanics directly on upper Fifteenmile Group rocks. Previously published radiometric ages from Macdonald et al. (2010, in press), Rooney et al (2014; 2015) , Strauss et al. (2014), Baldwin et al., (2016), Milton et al. (2017), Jefferson and Parrish (1989).

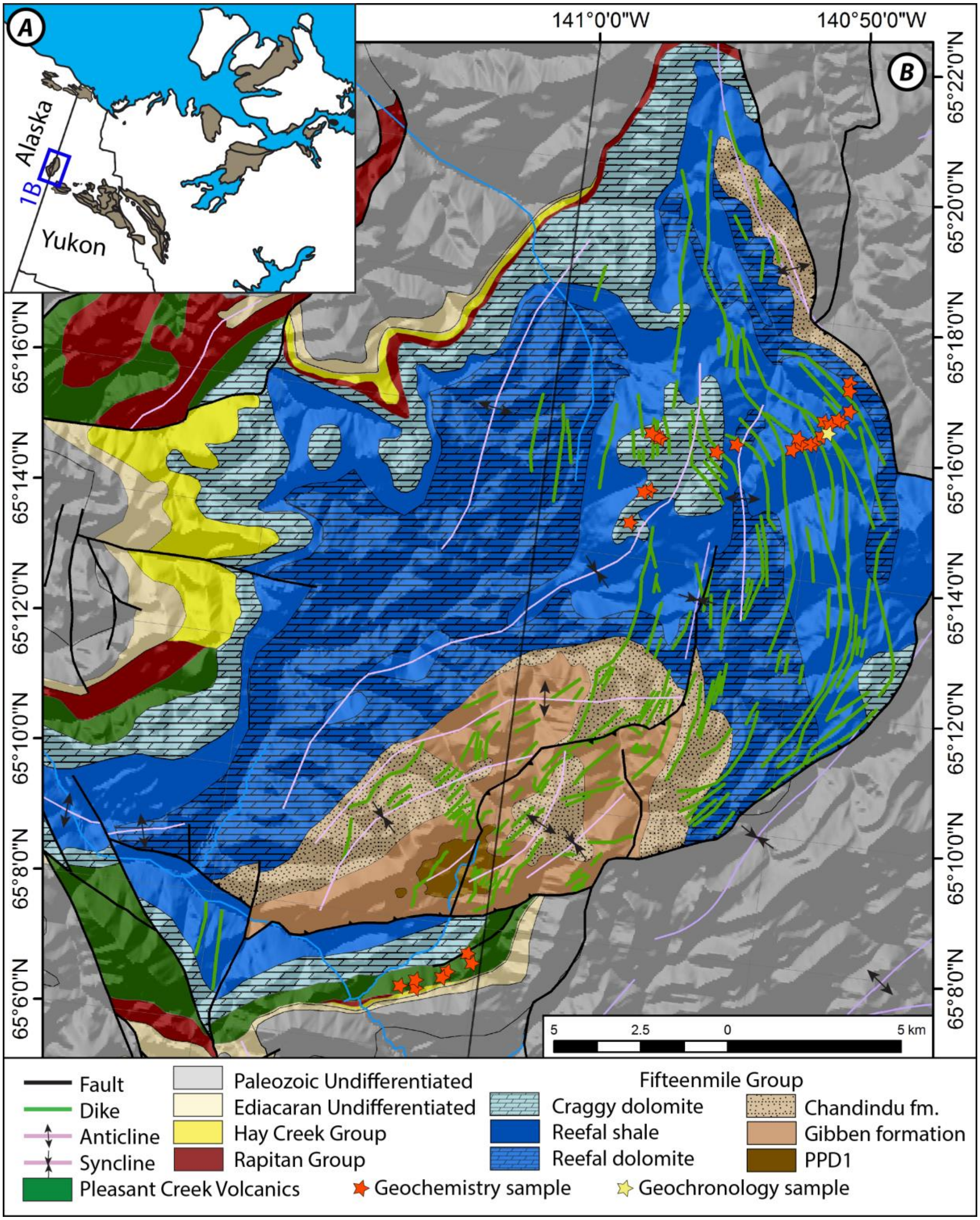

Figure 4. Regional map of the Tatonduk Inlier showing the distribution of Pleasant Creek Volcanics and Tatonduk Dykes.

Here we present a new $^{206}Pb/^{238}U$ ID-TIMS baddeleyite age of 713.7 ± 0.9 Ma on the Tatonduk Dykes, along with new petrographic and geochemical analyses on both the dykes and associated flows of the Pleasant Creek Volcanics. Although this mafic suite temporally overlaps the Franklin LIP, its compositions are distinct from those of the Franklin CFB, including associated radiating dyke swarms, sills and major volcanic flows. Specifically, the Tatonduk suite appears to represent melting of metasomatized sub-continental lithospheric mantle (SCLM). We propose that these rocks represent one end member in a continuum between Continental Flood Basalt (CFB) magmatism associated with the core of the Franklin LIP and younger rift-related volcanism that influenced a massive area of northern Laurentia during protracted break-up of the Rodinian supercontinent (Macdonald et al., 2017).

Regional Geology

Proterozoic rocks of the Yukon block outcrop in a series of inliers that span central Yukon in northwestern Canada: the Wernecke, Hart River, Coal Creek, and Tatonduk inliers (Fig. 3). These inliers comprise Proterozoic strata that have historically been subdivided into three sequences (A, B, C; Rainbird et al., 1996). Sequence A strata include the ca. 1.6 Ga Wernecke Supergroup. Sequence B includes Tonian-aged strata of the Mackenzie Mountain Supergroup, and Sequence C strata include the latest Tonian to early Paleozoic Windermere Supergroup (Fig. 3). Latest Tonian to earliest Cryogenian volcanic rocks and associated dykes occur in both the Coal Creek and Tatonduk inliers. A detailed discussion of ages and stratigraphic and tectonic context of the Mount Harper Volcanics in the Coal Creek inlier are given in Macdonald et al. (this volume). Recently acquired paleomagnetic data on the Mount Harper Volcanics imply that the Yukon block has rotated 55º counterclockwise relative to autochtonous Laurentia, most likely contemporaneous with deposition of Sequence C (Eyster et al., 2017). Rotation of the Yukon block, along with development of Sequence C basins, was likely linked to long-lived strike-slip displacement along the Cordilleran margin (Eyster et al., 2017; Strauss et al., 2015) preceding full opening of the margin and initiation of a passive margin in the latest Ediacaran to early Cambrian (Colpron et al., 2002; Macdonald et al., this volume).

The Tatonduk inlier is the westernmost of the inliers and straddles the Yukon-Alaska border (Fig. 3). Here, strata of what were previously assigned to the upper part of the Lower Tindir Group (Young, 1982) were reassigned by Macdonald et al. (2011) to the Fifteenmile Group, which unconformably overlies older strata inferred to be the equivalent of the Pinguicula Group (formerly included in the lower part of the Lower Tindir Group). The Fifteenmile Group is in turn unconformably overlain by the Cryogenian Pleasant Creek Volcanics, Rapitan Group, and Hay Creek Group. These, together with the Ediacaran, informal "Upper Group" (Macdonald et al., this volume), were previously ascribed to the Upper Tindir Group (Young, 1982). The late Tonian (ca. 755–717 Ma) Mount Harper Group, which is prominent in the Coal Creek inlier, is entirely absent in the Tatonduk inlier, such that the basal Cryogenian disconformity here represents a significant depositional hiatus.

The Pleasant Creek Volcanics occur directly above this disconformity and comprise a succession up to 330 m thick of basaltic to intermediate massive, pillowed lava flows, and volcanoclastic breccia (Young, 1982); Macdonald et al., this volume). The Pleasant Creek Volcanics are locally overlain by or interfinger with glaciomarine rocks of the Rapitan Group (Young, 1982). Due to poor exposure, the exact nature of this relationship is difficult to determine. Regionally, all of these units are unconformably overlain by breccia of the Hay Group (Macdonald et al., this volume). Although the contact between the Pleasant Creek Volcanics and Rapitan Group is nowhere exposed, clasts derived from the underlying Pleasant Creek Volcanics occur in the lowermost Rapitan strata (Macdonald et al., this volume). These strata dominantly consist of finely laminated mudstone and siltstone with scattered lonestones and dropstones and prominent intervals of hematitic siltstone and jaspilitic iron formation (Cox et al., 2016a; Young, 1982); Macdonald et al., this volume). Paleocurrents in the Rapitan Group and stratigraphic geometries indicate a west-facing margin (in current coordinates; Young, 1982).

The Pleasant Creek Volcanics are considered equivalent to the Tatonduk dykes, which cross-cut the Fifteenmile Group strata and form a roughly north-south dyke swarm over an area of ~200 km^2 to the north of the Yukon Thrust (Fig. 3). Arcuate folding of the dykes is thought to be related to Jurassic displacement on the Yukon thrust. The original unfolded orientation of the dykes is unclear, but in present coordinates, it could range anywhere from 310º to 30º. Taking into consideration the apparent 55º counterclockwise rotation of the Yukon block relative to autochtonous Laurentia (Eyster et al., 2017), it is unlikely that the original dyke swarm paralleled the trend of the Franklin dyke swarm.

Petrography of the Pleasant Creek Volcanics and Tatonduk Dykes

High MgO samples are characterized by euhedral to subhedral olivine (Fig. 4A-B), euhedral to subhedral clinopyroxene and sub-ophitic plagioclase laths (Fig. 4C-D). Minor phases include orthopyroxene, Fe-Ti oxides and rutile. Low MgO samples contain phenocrystic clinopyroxene (Fig. 4G), abundant plagioclase found as a groundmass mesh (Fig. 4G) and very fine-grained biotite (Fig. 4F). Volcanic samples contain glass along with glomeroporphyritic plagioclase and olivine (Fig. 4H-I). Mineral relationships suggest a crystallizing sequence of olivine, followed by clinopyroxene and plagioclase then biotite.

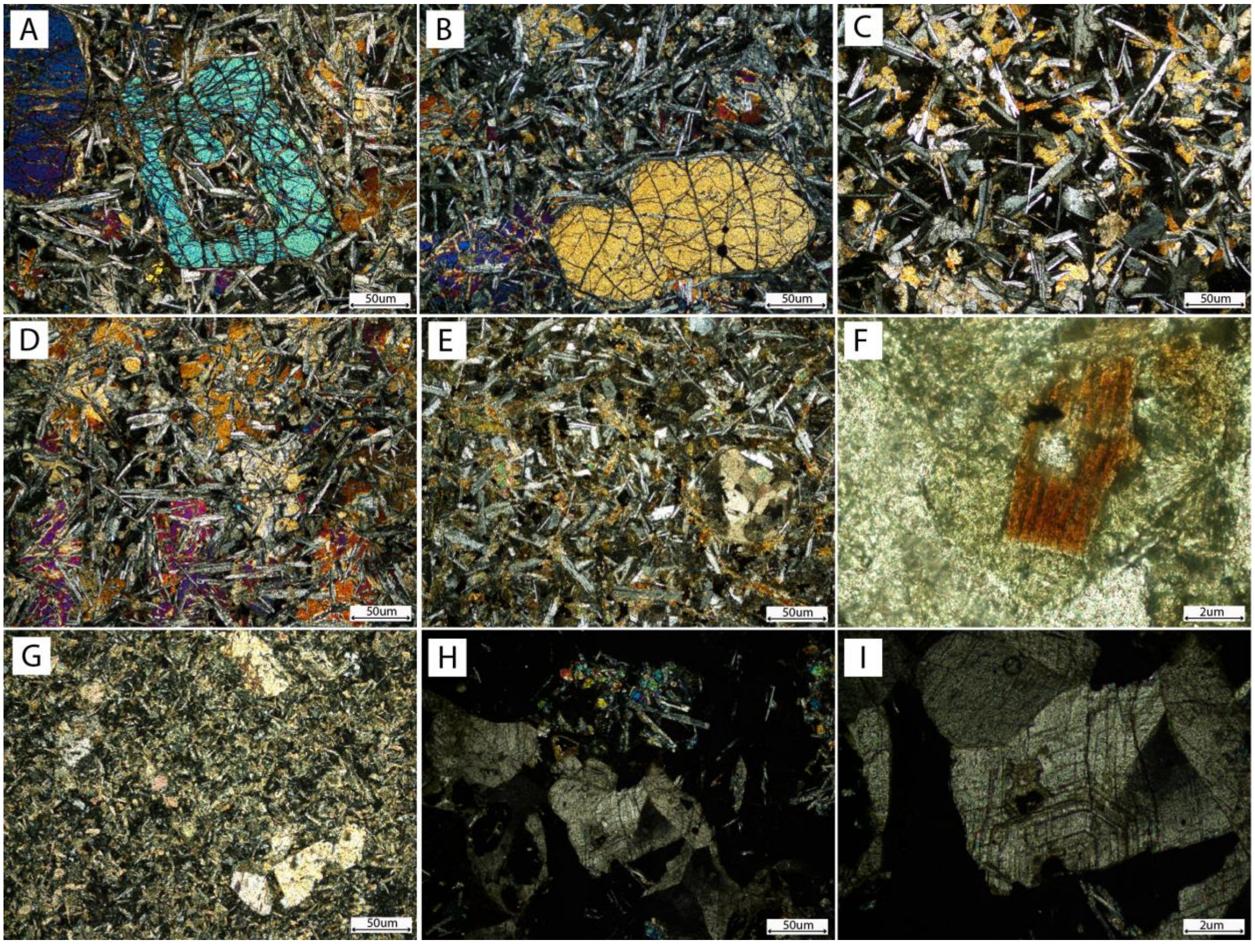

Figure 5 (A-B) Phenocrystic olivine including hopper varieties and clinopyroxene crystals with sub-ophitic plagioclase laths (x-polar). (C) Clinopyroxene and sub-ophitic plagioclase laths in a dark indistinguishable groundmass (x-polar). (D) Large clinopyroxene and sub-ophitic plagioclase laths. (E) Infilled vesicle surrounded by plagioclase, clinopyroxene and very fine grained biotite (x-polar). (F) Subhedral biotite (p-polar). (G) Large plagioclase, glass and glomeroporphyritic plagioclase and olivine. (H) Zoned plagioclase and glass.

Geochronology

Five baddeleyite crystals were analyzed from sample TI11-010, a course grained basaltic dyke (Table X, Fig. 6). Calculated weights were estimated using photomicrographs of selected grains, and are between 0.1 and 0.3 µg, with calculated U concentrations between 96 and 250 ppm. Th/U ratios are typically low in baddeleyite, and these analyses indicated Th/U ratios between 0.03 and 0.04, with one at 0.21. All data are concordant and the oldest four analyses form a coherent age cluster (Fig. 6) with one younger analysis, indicating the effect of Pb loss for that crystal. The coherence of the four older data argues against disturbance and Pb loss and support our interpretation of the crystallization age corresponding to the older cluster. The weighted-mean $^{206}Pb/^{238}U$ age is presented here as the low abundance and relatedly larger analytical uncertainties in the measurement of ^{207}Pb and ^{235}U means that more meaningful age data are provided by the $^{206}Pb/^{238}U$ system. The weighted mean $^{206}Pb/^{238}U$ age of the older four analyses is 713.7 ± 0.9 Ma (2σ, MSWD = 0.13, n = 4), taken as the preferred age for dyke crystallization.

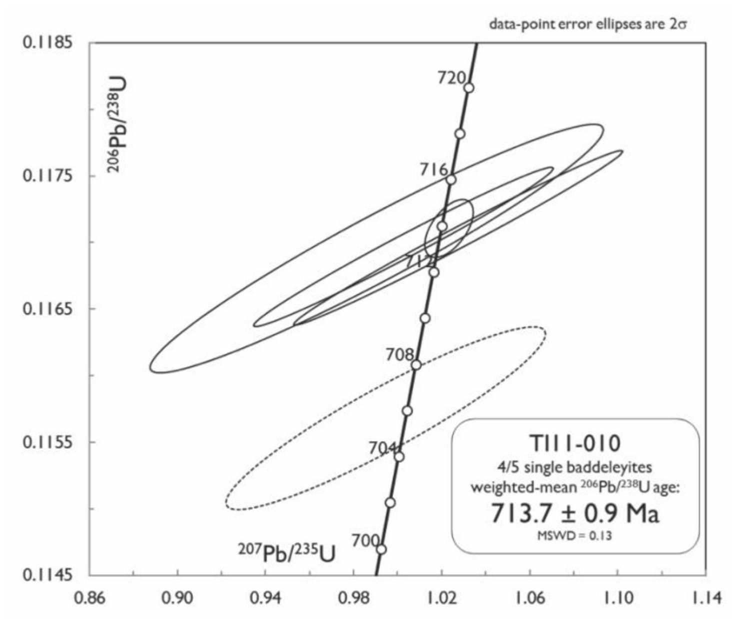

Figure 6. Concordia plot of U-Pb data for Tatonduk dyke sample TI11-010. Dashed ellipse denotes datum not included in the weighted-mean $^{206}Pb/^{238}U$ age.

Geochemistry

The Pleasant Creek Volcanics and Tatonduk Dykes range in composition from basalt through andesite, but the majority have K_2O concentrations that classify them as shoshonites (Fig. 7A) The most primitive composition observed has an MgO content of ~9%, and Mg# are elevated across all compositions, ranging from 72 at basaltic compositions to 58 at andesitic compositions (Fig. 7B). Major element cross plots show broadly coherent major element variations, and Fe and Ti show little to no enrichment with decreasing Mg, typical of calc-alkaline magmatism (Fig. 8). Aluminum concentrations are invariant and average 15%, indicating that Al was buffered with respect to the crystallisation of plagioclase.

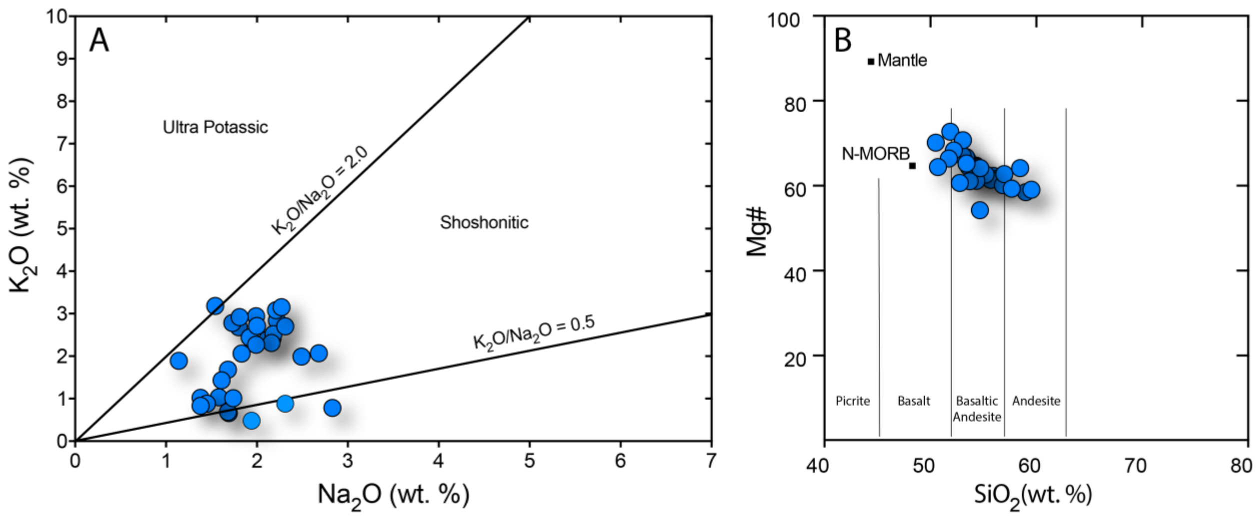

Figure 7. (A) K_2O vs. Na_2O showing potassic enrichment into the field of shoshonitic compositions. (B) Mg# vs. SiO_2 revealing the high Mg# across all compositions.

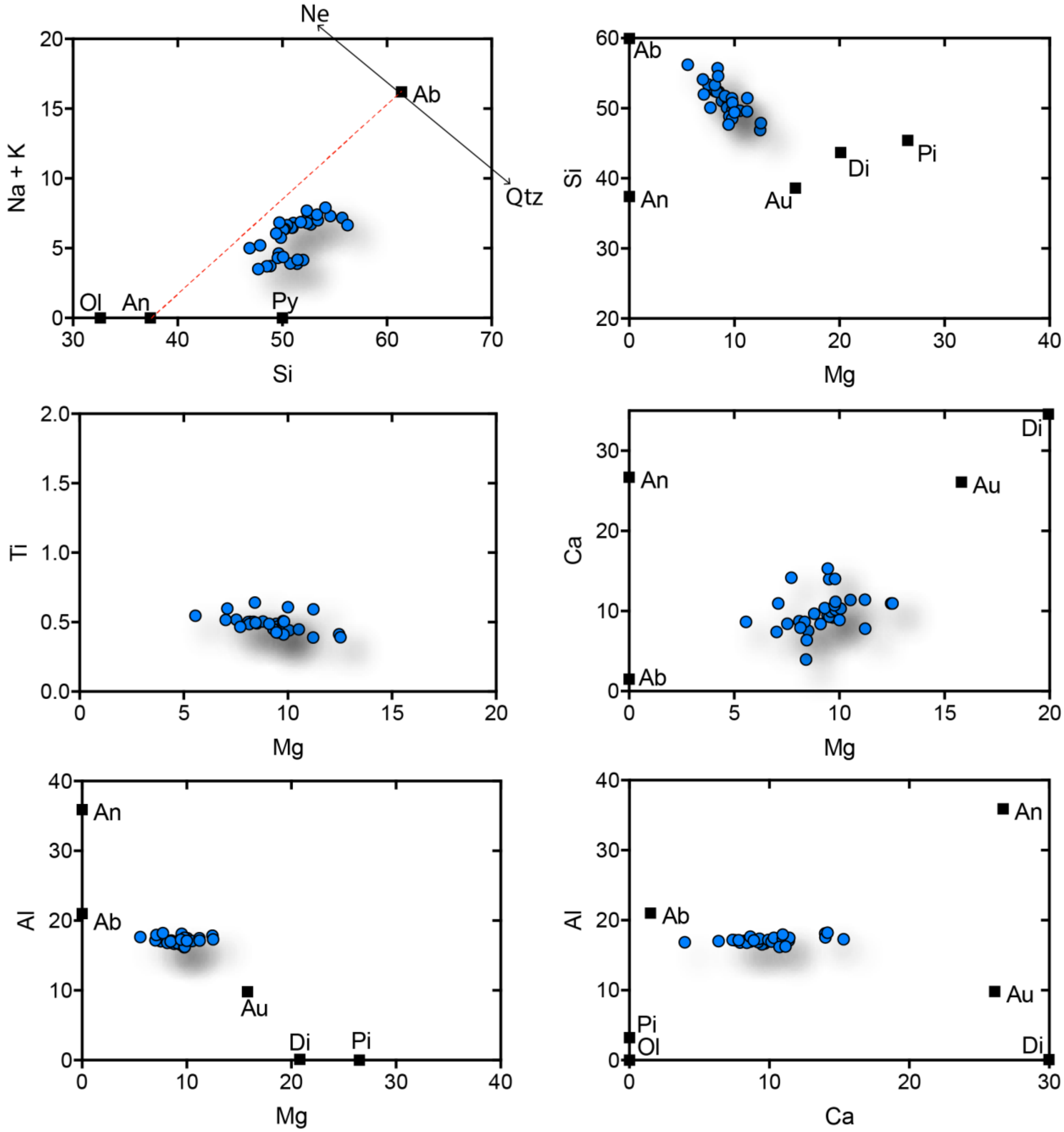

Figure 8. Major element cation plots along with mineral compositions. Blue field are the compositions produced via fractional crystallization of a water-saturated melt between 0.1 to 5 kb. Black line is the liquid line of descent for anhydrous fractional crystallization at 0.1kb. Compositions were calculated using alphaMELTS (Smith and Asimow, 2005). Ol = Olivine, Pi = Pigeonite, Au = Augite, Bi = Biotite, ph = phlogopite, En = Enstatite, Di = Diopside, Py = Pyroxene, Pyr = Pyrope, Or = Orthoclase, Al = Albite, An = Anorthite.

From a trace element perspective, the lavas and dykes are enriched in large ion lithophile elements (LILE) and light rare earth elements (LREE: La-Ce-Pr) and have flat middle rare earth element (MREE) concentrations (Fig. 9A). The heavy rare earth elements (HREE), which are sensitive to residual garnet, are distinctly unfractionated, with low Sr/Y (Ave. = 4.78) and $(La/Yb)_N$ (Ave. = 5.2) ratios indicative of melts that did form in equilibrium with residual garnet. Pronounced Ti and Nb depletions are evident, are largely invariant, and are difficult to reconcile with either crustal assimilation or mixing (Fig. 9B-C). Isotopically, these lavas and dykes are highly evolved with average $\varepsilon_{Nd(t=713)}$ compositions of -10.9. Similar to Nb anomalies, the evolved isotopic character is largely decoupled from variations in incompatible element abundances (Fig. 9D). Considering the unfractionated MORB-like Nd and Sm concentrations (Fig. 9A), these isotopic enrichments must be old to allow for the significant ingrowth of radiogenic Nd.

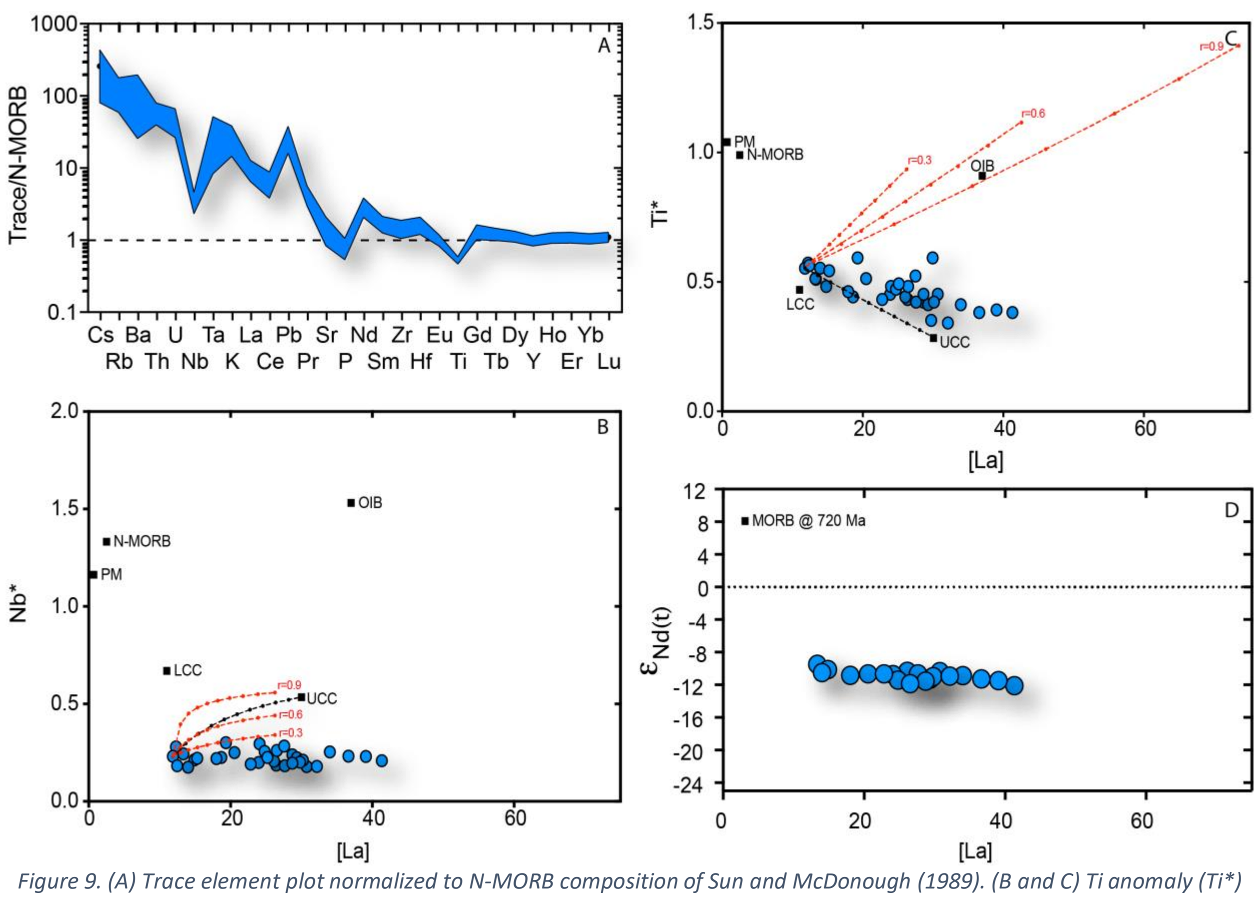

Figure 9. (A) Trace element plot normalized to N-MORB composition of Sun and McDonough (1989). (B and C) Ti anomaly (Ti) and Nb anomaly (Nb*) where $Nb^* = Nb_N / sqrt(U_N \times La_N)$ and $Ti^* = Ti_N / sqrt(Eu_N \times Gd_N)$ and N subscript denotes that all elemental concentrations have been normalized to bulk earth (CHUR). Dashed red lines are assimilation and fractional crystallization models based on a fractionating mineral assemblage of 11% olivine, 30% plagioclase and 60 % clinopyroxene resulting in bulk distribution coefficients of: $D_{Ti} = 0.254$, $D_{Nb} = 0.127$, $D_U = 0.027$, $D_{La} = 0.31$, $D_{Gd} = 0.92$, $D_{Eu} = 1.20$. R values are the ratio of assimilation to fractional crystallization. The mineral assemblage was determined from alphaMELTS modelling (Smith and Asimow, 2005). Dashed black line is simple mixing with the upper continental crust. N-MORB = Normal Mid Ocean*

Ridge Basalt, OIB = Ocean Island Basalt, PM = Primitive Mantle and are from Sun and McDonough (1989). UCC = Upper Continental Crust and LCC = Lower Continental Crust and are from Taylor and McLennan (1995). (D) Epsilon Nd ($\varepsilon_{Nd(t)}$) vs. La with $\varepsilon_{Nd(t)}$ calculated at 713 Ma.

Petrogenesis

The spectrum of observed major element compositions along with the observed mineralogy are most consistent with low pressure fractional crystallisation of a water-rich melt resulting in a fractional crystallisation sequence of olivine → clinopyroxene + plagioclase → clinopyroxene + plagioclase + biotite. Calculated phase diagrams for the parental and evolved melt supports this crystallisation sequence illustrating that primitive compositions will fractionate olivine then co-crystallise clinopyroxene and plagioclase (Fig. 10A), while the more evolved compositions should crystallise clinopyroxene, plagioclase and late biotite (Fig. 10B).

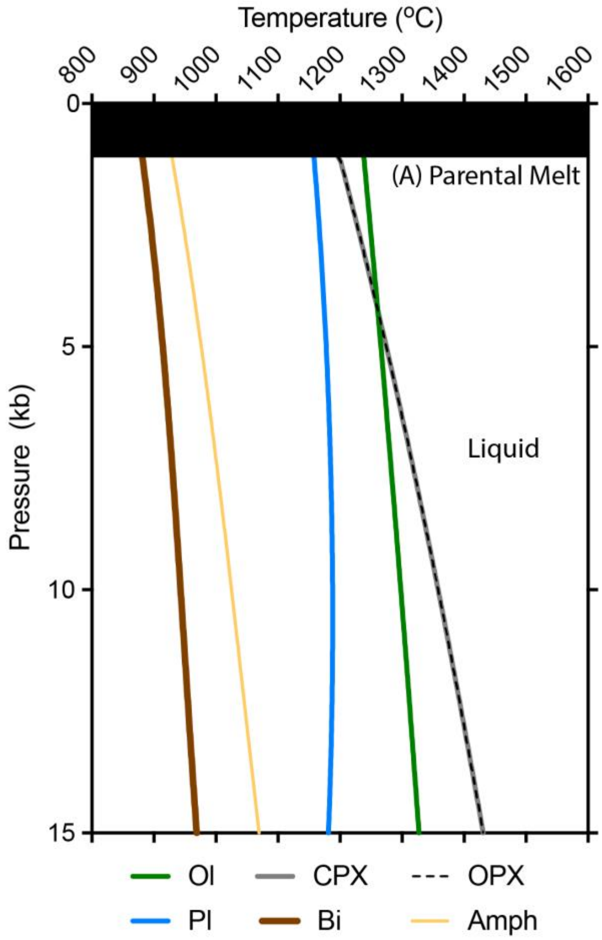

Figure 10. (A) Phase diagram for the most primitive (Parental) melt of the Pleasant Creek Volcanics and Tatonduk Dykes (MgO (wt.%) = 9%, Mg# = 72, Fo88). (B) Phase diagram for the most evolved melt of the Pleasant Creek Volcanics and Tatonduk Dykes (MgO (wt.%) = 6%, Mg# = 57, Fo77).

While the suite as a whole spans the spectrum of basalts to andesites, the andesites in particular have relatively high Mg#. Notable examples of high Mg# andesites include *sensu stricto* boninites (Crawford et al., 1989) as well as low-silica adakites (Castillo, 2006; Kelemen et al., 2013). It is generally thought that high Mg# andesites cannot be formed by melting of fertile mantle followed by protracted assimilation and/or fractional crystallization. For example, Kushiro (1969) showed experimentally that anhydrous melting of lherzolite could not produce a primary andesite. Furthermore, the addition of water had the effect of higher SiO_2 but with MgO offset lower than their anhydrous equivalents. Consequently, high Mg# andesites could not be obtained. This result has also been shown in more complex systems incorporating the effects of

CO_2 as well as H_2O (Liu et al., 2006). Falloon and Danyushevsky (2000) showed that melting of hydrated harzburgite at low pressures could produce a high Mg# andesite (*sensu stricto* boninites) while low-silica adakites are generated by melting of a mafic precursor followed by reaction with and melting of peridotite (Rapp et al., 1999; Rapp and Watson, 1995).

The Tatonduk suite of high Mg# andesites does not fit into the above categories; low Sr/Y and low $(La/Yb)_N$ ratios are inconsistent with low-silica adakites, whereas the lack of a U-shaped REE profile (Cameron et al., 1983; Hickey and Frey, 1982; Kim and Jacobi, 2002) and a coherent liquid line of descent from basalts distinguishes them from boninites. Wood and Turner (2009) more recently showed that melting of hydrated depleted peridotite will produce high Mg# parental liquids (picrites), with both MgO and SiO_2 increasing in tandem with increasing unsaturation of peridotite in clinopyroxene, up to pressures of at least 6kb. Perhaps unsurprisingly, the most primitive composition observed in the Tatonduk suite (Mg# = 72 / Fo88) would seem to be in equilibrium with a peridotitic assemblage at ~5kb (Fig. 10A). Consequently the primary melt for the Pleasant Creek Volcanics and Tatonduk Dykes may be a result of the relatively low pressure melting of hydrated depleted peridotite.

Evidence for a major-element depleted source is also apparent, for example, in comparisons of these lavas and dykes with mid-ocean ridge basalts (MORB) at a common 8% MgO. This comparison shows that this suite of lavas and dykes has comparatively high SiO_2, low CaO, low Na_2O and high Mg#. Low FeO and low TiO_2 are also apparent but likely reflect the combination of a depleted source and the calc-alkaline nature of the suite. Given a lherzolite source for MORB (Workman and Hart, 2005), such systematic differences are consistent with a mantle source depleted in major elements (Klein and Langmuir, 1987; Turner and Hawkesworth, 1995), as would be expected with undersaturation of clinopyoxene in the mantle source.

Table 1. Comparisons between the Pleasant Creek Volcanics and MORB at a common 8% MgO. MORB data is from Jenner and O'Neill (Jenner and O'Neill, 2012).

	Pleasant Creek Volcanics	MORB
SiO_2	53.22	50.5
TiO_2	0.63	2.83
Al_2O_3	15.73	15.66
FeOT	8.03	10.93
Mg#	0.67	0.59
CaO	10.53	11.85
Na_2O	1.90	2.46
K_2O	1.71	0.11
P_2O_5	0.09	0.12
Ce/Pb	7.27	30.6
Nb/U	3.94	46.4
Nb/La	0.32	0.77
Ti/Zr	43.40	140.95
eNd @ 720 Ma	-12.0	N/A
Depleted Source		
Enriched Source		

We suggest that the high Mg# character of this suite is a direct result of the primary melt being derived from a peridotite that was undersaturated in clinopyroxene. Furthermore, the development of high-Mg# andesites is a direct result of this initial high Mg# primary melt followed by the fractionation of a low Mg# gabbroic assemblage (Fig. 11), dominated by plagioclase and clinopyroxene ± biotite.

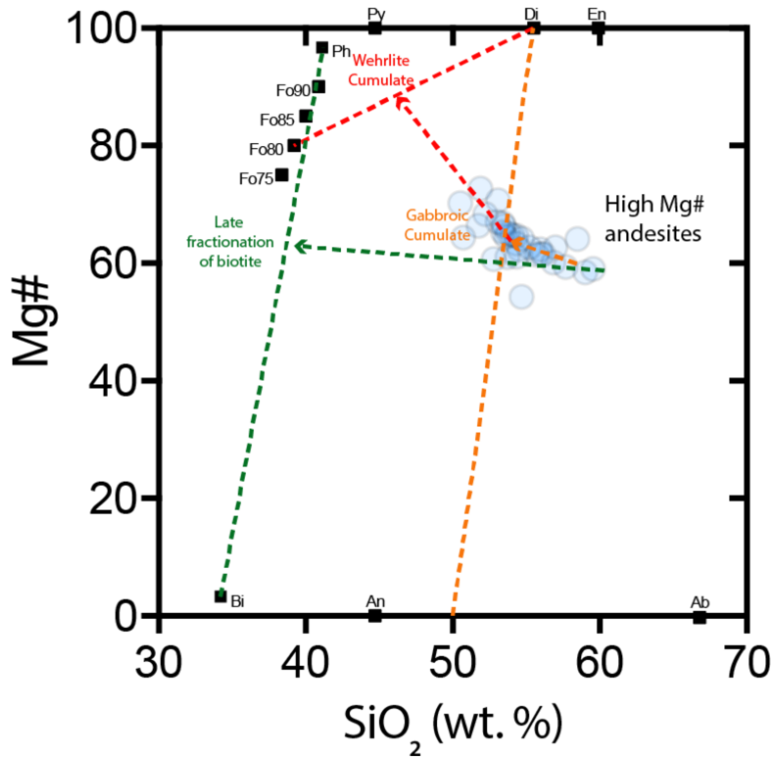

Figure 11. Mg# vs. SiO_2. Red dashed line is a vector consistent with fractionation of a wehlite assemblage, orange dashed line represents fractionation of gabbroic assemblage while green dashed line is fractionation of gabbroic assemblage plus biotite.

In contrast to the major element depletion, enrichment in K_2O, LILE, LREE and an evolved isotopic character are also apparent (Table 1, Fig. 9A). The invariant isotopic character and Nb anomalies (Fig. 9B-D) indicate only a minor role for upper crustal assimilation or mixing, despite significant LILE and LREE enrichment (Fig. 9A). This conclusion is supported by trace element modeling, which shows that assimilation of continental crust is incompatible with the observed trace element compositions (Fig. 9B-C).

Due to the lack of upper crustal assimilation involved in the petrogenesis of the Tatonduk suite, characteristics such as K_2O and trace element enrichment, large Nb and Ti depletions, along with a highly evolved isotopic character, must be related to the composition of the mantle source. Fractionation and assimilation from either a trace element-depleted or enriched source along a typical mantle array cannot produce the observed compositions (Fig. 12). Th/Yb and

Nb/Yb relationships (Fig. 12), combined with the requirement for significant ingrowth of radiogenic Nd would suggest early trace element enrichment of the mantle source followed by melting at 713 Ma. The age of this trace element enrichment is possibly constrained by a Nd/Sm pseudochron age of 1437 ± 23 (Fig. 13).

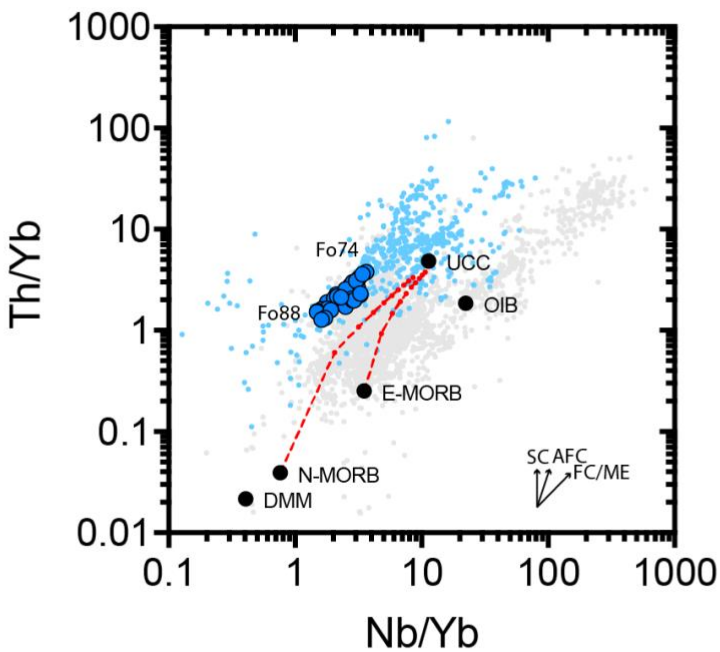

Figure 12. Th/Yb and Nb/Yb systematics after Pearce (2008). Grey dots are compositions of typical CFB while light blue dots are shoshonites. Dashed red lines are assimilation and fractional crystallization models based on a fractionating mineral assemblage of 11% olivine, 30% plagioclase and 60 % clinopyroxene assimilating UCC (r = 0.9). UCC = Upper Continental Crust (Taylor and McLennan, 1995), OIB = Ocean Island Basalt, E-MORB = Enriched Mid Ocean Ridge Basalt, N-MORB = Normal Mid Ocean Ridge Basalt (Sun and McDonough, 1989), DMM = Depleted MORB Mantle (Workman and Hart, 2005), SC = Subduction component, AFC = Assimilation and Fractional Crystallisation, FC = Fractional Crystallisation, ME = Mantle Enrichment. CFB and shoshonite data is from the Earthchem database (http://earthchem.org).

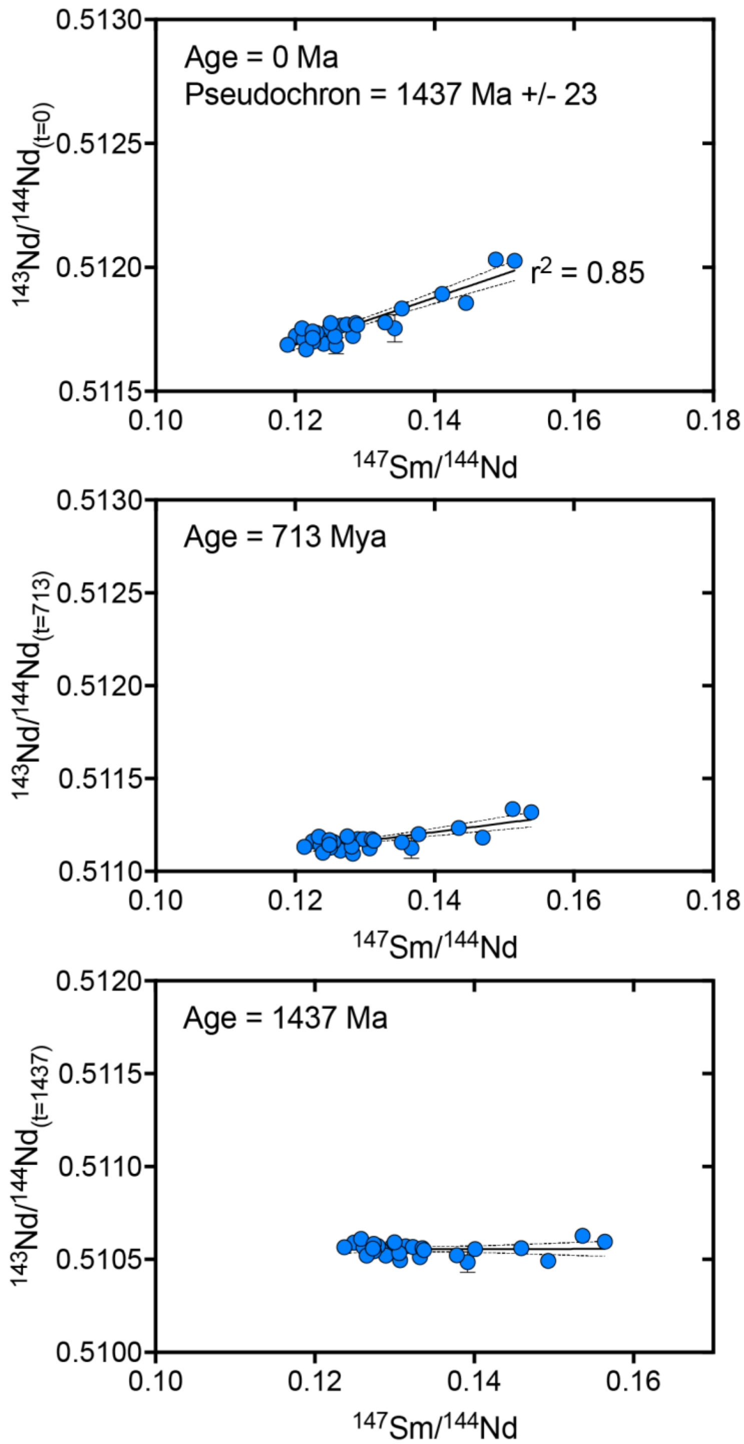

Figure 13. $^{143}Nd/^{144}Nd$ vs. $^{147}Sm/^{144}Nd$ at 0, 713 and 1437 Ma. The flat regression of the data at 1437 Ma corresponds to the calculated present day isochron age.

Comparison with Continental Flood Basalts of the Franklin Large Igneous Province

Igneous rocks associated with the Franklin LIP in northern Canada are dominated by basalt to basaltic andesites (i.e. continental tholeiites) (Bedard et al., 2016; Dostal et al., 1986), typical of most continental flood basalts and can be found as major flows, dykes and sills on Victoria Island (Bedard et al., 2016; Dostal et al., 1986), major flows in Arctic Alaska (Cox et al., 2015), along with numerous sills (e.g., Shellnutt et al., 2004) and dykes throughout northern mainland Canada and Greenland (Denyszyn et al., 2009a; Denyszyn et al., 2009b).

We use Ni/Mg and Sc/Fe ratios to explore similarities and differences between the Franklin LIP and the Tatonduk suite. Whereas both ratios are affected by assimilation and fractional crystallisation, magmatic rocks formed in different tectonic settings are delineated by this approach (Fig. 14A) because the ratios reflect differing mantle sources and degrees of partial melting. For example, Ni/Mg ratios are strongly governed by the modal abundance of olivine in the melt source and the contribution of olivine to the melt because olivine has a greater affinity for Ni than orthopyroxene, clinopyroxene, garnet or spinel. Generally, high Ni/Mg ratios in primitive melts reflect either a greater contribution of olivine to the melt (through higher degrees of melting or melting of harzburgite) or melting of garnet pyroxenite (Sobolev et al., 2005).

In contrast to Ni, Sc is incompatible in olivine and orthopyroxene and strongly compatible in garnet and clinopyroxene. As highlighted by Milidragovic and Francis (2016), Sc/Fe ratios are effective in discriminating between spinel and garnet peridotitic sources. When used in conjunction with Ni/Mg, three mantle end-members may be defined: spinel peridotite (high Sc/Fe, low Ni/Mg), garnet peridotite (low Sc/Fe, low Ni/Mg) and garnet pyroxenite (low Sc/Fe, high Ni/Mg). A fourth harzburgitic end-member may also be envisaged, which because it is depleted in iron and has a high modal abundance of olivine, would generate moderately high

Ni/Mg and moderately high Sc/Fe in harzburgite-derived basalts. These relationships control the distribution of basalts from differing tectonic settings as seen in Fig. 14A.

Figure 13 B-C shows that Ni/Mg and Sc/Fe ratios of both the Franklin CFB Tatonduk suite display significant variability, much of which can be explained by assimilation and fractional crystallisation. However, differences in Ni/Mg and Sc/Fe ratios persist even at primitive compositions, which suggests that much of these differences are inherited feature from their respective mantle sources. Back-calculation along their respective liquid lines of descent highlights these differences (Fig. 14A-B-C). The Pleasant Creek Lavas and Tatonduk Dykes are characterised by high Ni/Mg and moderately high Sc/Fe, suggesting derivation from a harzburgitic source. Considering their enrichment in potassium and trace elements and evolved isotopic signatures, we argue the likely harzburgitic source was metasomatised Laurentian sub-continental lithospheric mantle. In contrast, the basal Franklin lavas and flood cycle lavas define endmembers between spinel lherzolite and garnet lherzolite, consistent with the polybaric melting within the plume source envisaged for these CFB— fertile asthenospheric mantle.

It is evident that the major, trace and isotopic differences between the Franklin CFB and suite are not merely a consequence of calc-alkaline versus tholeiitic fractionation trends but reflect different mantle sources.

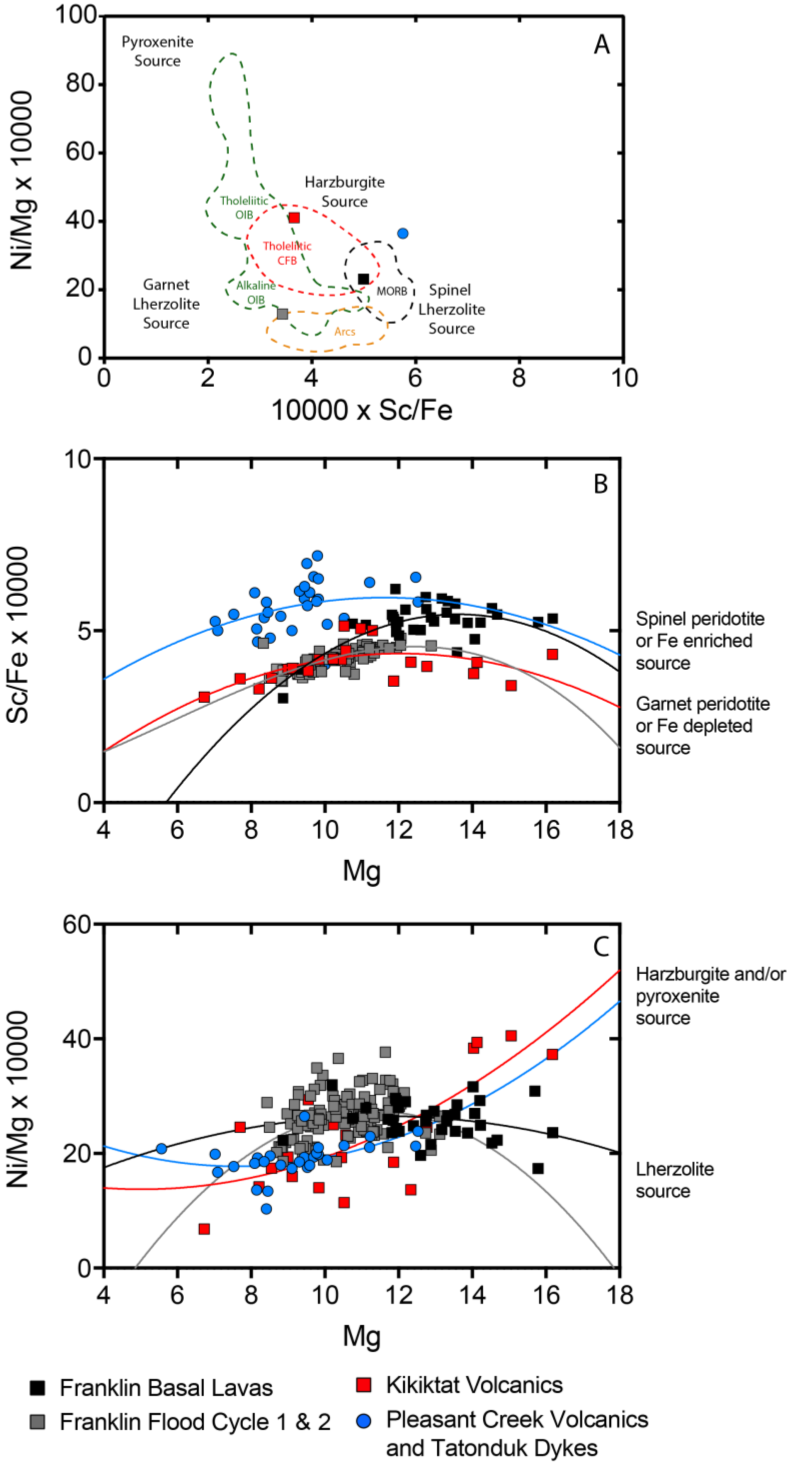

Figure 14. (A) 10000 x Ni/Mg vs. 10000 x Sc/Fe. Fields are calculated from kernel density estimates of ocean island basalts (OIB), continental flood basalts (CFB) and continental arcs (Arcs) from the EarthChem database (http:// http://www.earthchem.org). MORB data is from Jenner and O'Neill (2012). Filled squares and circles are the estimates of 10000 x Ni/Mg and 10000 x Sc/Fe calculated at 16% Mg for each respective volcanic suite. (B) 10000 x Sc/Fe vs. Mg defining liquid line of descents for the Franklin basalt lavas (black squares and black line), Franklin flood cycle 1 and 2 (grey squares and grey line) and the Pleasant Creek Volcanics and Tatonduk Dykes (blue circles and blue line). (C) 10000 x Ni/Mg vs. Mg defining liquid line of descents for the

Franklin basalt lavas (black squares and black line), Franklin flood cycle 1 and 2 (grey squares and grey line) and the Pleasant Creek Volcanics and Tatonduk Dykes (blue circles and blue line). Lines in both (B) and (C) are best fit polynomials.

Late Tonian–Cryogenian Magmatism in Yukon

The 713.7 ± 0.9 Ma Tatonduk suite represents but one of a series of latest Tonian to middle Cryogenian magmatic events along the Cordilleran margin, spanning from the Tatonduk inlier to central Idaho. For example, the nearby Mount Harper Volcanics in the late Tonian Mount Harper Group in the Coal Creek inlier (Fig. 3) are well dated; along with flows in the overlying Eagle Creek Formation of the Rapitan Group, magmatism spanned from >718.1 to 716.5 Ma (Fig. 3; Macdonald et al., this volume). The Mount Harper Volcanics represent the culmination of a stretching event that began > 750 Ma and presumably influenced the whole of the Yukon block. The ca. 750–717 Ma Callison Lake Formation and its equivalent Coates Lake Group in the Mackenzie Mountains (Fig. 3) were both deposited in discrete, normal fault-bound basins, likely the product of a long-lived strike system that might have influenced the entire western margin of Laurentia from the late Tonian until the middle Ediacaran (Strauss et al., 2015). The overlying Seela Pass Formation records alluvial fan deposition on the hanging wall of the north-dipping Mount Harper Fault (Mustard, 1991; Mustard and Roots, 1997) and is transitional above with the Mount Harper Volcanics. Hence the ca. 718.1–716.5 Ma calk-alkaline magmatism (Fig. 15) in the Coak Creek inlier is robustly linked to a continental-rift setting.

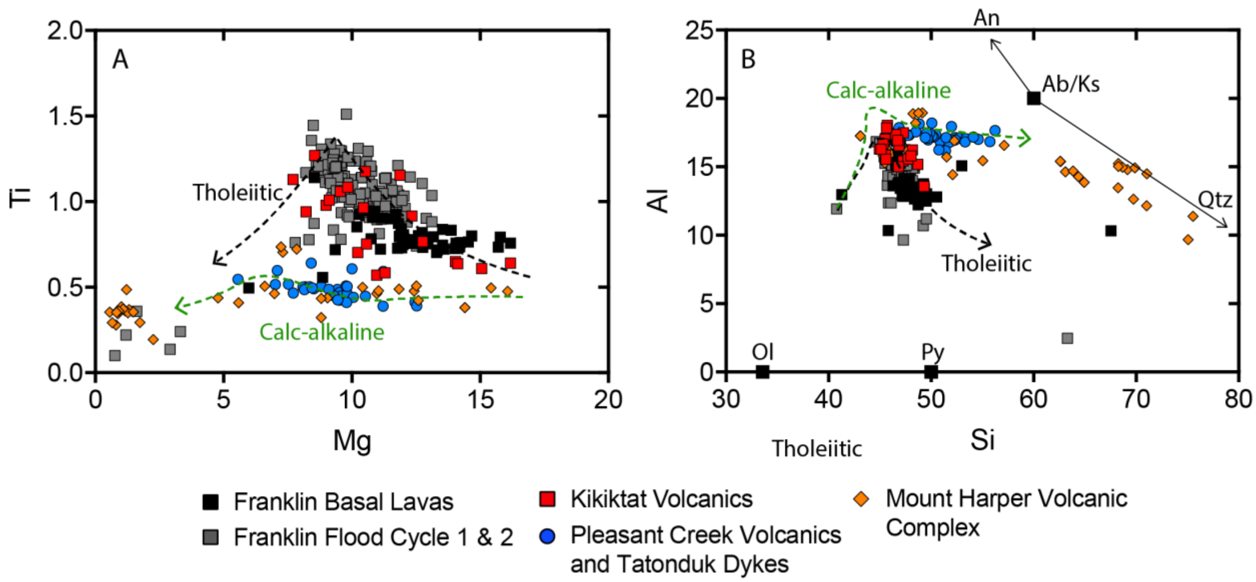

Figure 15.

Like the Mount Harper Volcanics, the the Tatonduk suite rocks fall on a distinctly calk-alkaline trend, rather than the more typical continental tholeiite trend typical of continental floods basalts such as the Franklin CFB (Fig. 15). Tatonduk magmatism is most parsimoniously interpreted to be the product of decompression melting of a metasomatized subcontinental mantle lithosphere, which implies that the magmatism was linked to continental extension. Whereas stratigraphic evidence of rifting coeval with volcanism is less straightforward in the Tatonduk inlier than in the Coal Creek inlier, the complete absence of strata equivalent to the late Tonian Mount Harper Group and significant erosional truncation of the underlying Fifteenmile Group in the Tatonduk inlier is consistent with local block rotation and uplift. Furthermore, the inferred w-facing basin margin during deposition of the Rapitan Group parallels the broad N-S trend of the Tatonduk dykes (Fig. 4). The implication is that the orientation of the Tatonduk dykes was the result of E-W extension (present day co-ordinates) rather than domal uplift and a radiating stress field expected of a mantle plume.

We do not preclude a role for the Franklin plume in the petrogenesis of the Pleasant Creek Volcanics and Tatonduk dykes (or Mount Harper Volcanic Complex), as it is plausible that the Franklin plume may have contributed heat to melt Laurentian sub-continental lithospheric mantle. However, we suggest that in the case of the Pleasant Creek Volcanics and Tatonduk dykes, the parsimonous explanation is that melting is related to decompression melting of metasomatised mantle during east-west extension along the western Laurentian margin.

Conclusions

Although their 713.7 ± 0.9 Ma age is similar to other mafic suites associated with the Franklin plume event (Fig. 1), the Tatonduk dykes and Pleasant Creek Volcanics are >1200 km from the plume head hypothesized for the Franklin CFB. They also do not obviously align with the Franklin dyke trend, even considering likely 55º counterclockwise rotation of the Yukon block in the Cryogenian to early Ediacaran (Eyster et al., 2017). Major, trace and isotopic data on the Tatonduk suite further reveal a composition that is entirely unique from the Franklin CFB and most likely reflects melting of potassic- and trace element-enriched Sub-Continental Lithospheric Mantle. We interpret this magmatism to be the product of decompression melting as the result of continental extension in the Yukon block, consistent with similar aged calk-alkaline magmatism and normal faulting in the Coal Creek inlier to the east (Macdonald et al., this volume). Whereas a link to emplacement of the massive Franklin LIP and its associated effect on continental break-up cannot be ruled out, this study highlights the complexity in defining what constitutes a LIP. Indeed, the overlap in ages between plume- and rift-related magmatism in northern Canada may contribute to the apparent anonymously long duration for the Franklin LIP as compared to better studied Phanerozoic examples (Macdonald and Wordsworth, 2017).

The Tatonduk magmatic suite also provides another example of early Cryogenian magmatism that yield consistent age constraints for the onset of Sturtian glaciation with those from the Coal Creek Inlier (Macdonald et al., 2010; this volume). Furthermore, the age and stratigraphic relationship of the Pleasant Creek Volcanics provides a maximum age constraint on the timing of deposition of Sturtian-age iron formation that is similar to constraints from the Mackenzie Mountains (Baldwin et al., 2016) and further allies the this iron formation to widespread mafic magmatism at this time.

Acknowledgements

This project was inspired by Charlie Roots, who provided enthusiastic support and guidance to GMC, GPH, and FAM in their projects in the Yukon. GMC's involvement in this project was supported by a Natural Sciences and Engineering Research Council of Canada (NSERC) Vanier Fellowship. GPH acknowledges financial support for this project from the Yukon Geological Survey, NSERC Discovery and Northern Research grants, the Geoscience for Energy and Mapping (GEM2) program, and a Gledden Fellowship from the University of Western Australia.

References

Ariskin, A. A., Kostitsyn, Y. A., Konnikov, E. G., Danyushevsky, L. V., Meffre, S., Nikolaev, G. S., McNeill, A., Kislov, E. V., and Orsoev, D. A., 2013, Geochronology of the Dovyren intrusive complex, northwestern Baikal area, Russia, in the Neoproterozoic: Geochemistry International, v. 51, no. 11, p. 859-875.

Bedard, J. H., Rainbird, R. H., Baragar, W. R. A., Williamson, M.-C., Hulbert, L. J., Hayes, B., Lissenberg, C. J., Hryciuk, M., Wing, B., Prince, J., Beard, C., Weis, D., J., S., Dell'Oro, T. A., Williamson, N., Cousens, B., Ernst, R. E., Nabelek, P. I., Naslund, H. R., and Montjoie, R., 2016, Geochemical database of Franklin sills, Natkusiak Basalts and Shaler Supergroup rocks, Victoria Island, Northwest Territories, and correlatives from Nunavut and the mainland. : Geological Survey of Canada , Open File # 8009.

Cameron, W. E., McCulloch, M. T., and Walker, D. A., 1983, Boninite petrogenesis: Chemical and Nd-Sr isotopic constraints: Earth and Planetary Science Letters, v. 65, no. 1, p. 75-89.

Castillo, P. R., 2006, An overvew of adakite petrogenesis: Chinese Science Bulletin, v. 51, no. 3, p. 257-268.

Colpron, M., Logan, J. M., and Mortensen, J. K., 2002, U–Pb zircon age constraint for late Neoproterozoic rifting and initiation of the lower Paleozoic passive margin of western Laurentia: Canadian Journal of Earth Sciences, v. 39, p. 133-143.

Courtillot, V., Jaupart, C., Manighetti, I., Tapponier, P., and Besse, J., 1999, On causal links between flood basalts and continental breakup. : Earth and Planetary Science Letters, v. 166, p. 177–195.

Cox, G. M., Halverson, G. P., Poirier, A., Le Heron, D., Strauss, J. V., and Stevenson, R., 2016a, A model for Cryogenian iron formation: Earth and Planetary Science Letters, v. 433, p. 280-292.

Cox, G. M., Halverson, G. P., Stevenson, R. S., Vokaty, M., Poirier, A., Kunzmann, M., Li, Z.-X., Dudás, F. Ö., Strauss, J. V., and Macdonald, F. A., 2016b, Continental Flood Basalt Weathering as a Trigger for Neoproterozoic Snowball Earth: Earth and Planetary Science Letters, v. 446, p. 88-99.

Cox, G. M., Strauss, J. V., Halverson, G. P., Schmitz, M. D., McClelland, W. C., Stevenson, R. S., and Macdonald, F. A., 2015, Kikiktat volcanics of Arctic Alaska—Melting of harzburgitic mantle associated with the Franklin large igneous province: Lithosphere, v. 7, no. 3, p. 275-295.

Crawford, A. J., Falloon, T. J., and Green, D. H., 1989, Classification, petrogenesis and tectonic setting of boninites, London, Unwyn Hyman, Boninites and Related Rocks.

Denyszyn, S. W., Davis, D. W., and Halls, H. C., 2009a, Paleomagnetism and U–Pb geochronology of the Clarence Head dykes, Arctic Canada: orthogonal emplacement of mafic dykes in a large igneous province: Canadian Journal of Earth Sciences, v. 46, no. 3, p. 155-167.

Denyszyn, S. W., Halls, H. C., Davis, D. W., and Evans, D. A. D., 2009b, Paleomagnetism and U-Pb geochronology of Franklin dykes in High Artic Canada and Greenland: a revised age and paleomagnetic pole constraining block rotations in the Nares Strait region Canadian Journal of Earth Sciences, v. 46, p. 689-705.

Dostal, J., Baragar, W. R. A., and Dupuy, C., 1986, Petrogenesis of the Natkusiak continental basalts, Victoria Island, Northwest Territories, Canada: Canadian Journal of Earth Sciences, v. 23, no. 5, p. 622-632.

Ernst, R. E., Hamilton, M. A., Soderlund, U., Hanes, J. A., Gladkochub, D. P., Okrugin, A. V., Kolotilina, T., Mekhonoshin, A. S., Bleeker, W., LeCheminant, A. N., Buchan, K. L., Chamberlain, K. R., and Didenko, A. N., 2016, Long-lived connection between southern Siberia and northern Laurentia in the Proterozoic: Nature Geosci, v. 9, no. 6, p. 464-469.

Ernst, R. E., and Soderlund, U., 2012, A proposed 725Ma Dovyren-Kingash LIP of southern Siberia and possible reconstruction link with teh 725-715 Ma Franklin LIP of northern Larentia, Geological Association of Canada (GAC) - Mineralogical Association of Canada (MAC) Joint Annual Meeting, Geoscience at the Edge, May 27-29: St John's, Newfoundland and Labrador, Canada.

Ernst, R. E., Wingate, M. T. D., Buchan, K. L., and Li , Z. X., 2008, Global record of 1600-700 Ma Large Igneous Provinces (LIPs): Implications for the reconstruction of the proposed Nuna (Columbia) and Rodinia supercontinents: Precambrian Research, v. 160, p. 159-178.

Eyster, A. E., Fu, R. R., Strauss, J. V., Weiss, B. P., Roots, C. F., Halverson, G. P., Evans, D. A., and Macdonald, F. A., 2017, Paleomagnetic evidence for a large rotation of the Yukon block relative to Laurentia: Implications for a low-latitude Sturtian glaciation and the breakup of Rodinia: GSA Bulletin, v. 129, p. 38–58.

Falloon, T. J., and Danyushevsky, L. V., 2000, Melting of Refractory Mantle at 1.5, 2 and 2.5 GPa under Anhydrous and H2O-undersaturated Conditions: Implications for the Petrogenesis of High-Ca Boninites and the Influence of Subduction Components on Mantle Melting: J. Petrology, v. 41, no. 2, p. 257-283.

Halls, H. C., Hamilton, M. A., and Denyszyn, S. W., 2010, Paleomagnetism and U–Pb baddeleyite dating of the Melville Bugt and Ataa Sund dykes, Greenland: 6th International Dyke Conference, Dyke swarms: keys for geodynamic interpretation: Varanasi, India.

Heaman, L. M., LeCheminant, A. N., and Rainbird, R. H., 1992, Nature and timing of Franklin igneous events, Canada: Implications for a Late Proterozoic mantle plume and the break-up of Laurentia: Earth and Planetary Science Letters, v. 109, no. 1-2, p. 117-131.

Hickey, R. L., and Frey, F. A., 1982, Geochemical characteristics of boninite series volcanics: implications for their source: Geochimica et Cosmochimica Acta, v. 46, no. 11, p. 2099-2115.

Jefferson, C. W., and Parrish, R. R., 1989, Late Proterozoic stratigraphy, U-Pb ages, and rift tectonics, Mackenzie Mountains, northwest Canada: Canadian Journal of Earth Sciences, v. 26, no. 9, p. 1785-1802.

Jenner, F. E., and O'Neill, H. S. C., 2012, Analysis of 60 elements in 616 ocean floor basaltic glasses: Geochemistry, Geophysics, Geosystems, v. 13, no. 2, p. Q02005.

Kelemen, P. B., Yogodzinski, G. M., and Scholl, D. W., 2013, Along-Strike Variation in the Aleutian Island Arc: Genesis of High Mg# Andesite and Implications for Continental Crust, Inside the Subduction Factory, American Geophysical Union, p. 223-276.

Kim, J., and Jacobi, R., 2002, Boninites: characteristics and tectonic constraints, northeastern Appaachians: Physics and Chemistry of the Earth, v. 27, p. 109-127.

Klein, E. M., and Langmuir, C. H., 1987, Global Correlations of Ocean Ridge Basalt Chemistry with Axial Depth and Crustal Thickness: Journal of Geophysical Research, v. 92, no. B8, p. 8089-8115.

Kushiro, I., 1969, The system forsterite-diopside-silica with and without water at high pressures: American Journal of Science, v. 267A, p. 269–294.

Liu, X., O′ Neill, H. S. t. C., and Berry, A. J., 2006, The effects of small amounts of H2O, CO2 and Na2O on the partial melting of spinel lherzolite in the system CaO–MgO–Al2O3– SiO2 ± H2O ± CO2 ± Na2O at 1.1 GPa. : Journal of Petrology, v. 47, p. 409-434.

Macdonald, F. A., McClelland, W. C., Schrag, D. P., and Macdonald, W. P., 2009, Neoproterozoic glaciation on a carbonate platform margin in Arctic Alaska and the origin of the North Slope subterrane: Geological Society of America Bulletin, v. 121, no. 3-4, p. 448-473.

Macdonald, F. A., Schmitz, M. D., Crowley, J. L., Roots, C. F., Jones, D. S., Maloof, A. C., Strauss, J. V., Cohen, P. A., Johnston, D. T., and Schrag, D. P., 2010, Calibrating the Cryogenian: Science, v. 327, no. 5970, p. 1241-1243.

Macdonald, F. A., Smith, E. F., Strauss, J. V., Cox, G. M., Halverson, G. P., and Roots, C. F., 2011, Neoproterozoic and early Paleozoic correlations in the western Ogilvie Mountains, *in* MacFarlane, K. E., Weston, L. H., and Blackburn, L. R., eds., Yukon Exploration and Geology, p. 161-182.

Merdith, A. S., Collins, A. S., Williams, S. E., Pisarevsky, S., Foden, J. F., Archibald, D., Blades, M. L., Alessio, B. L., Armistead, S., Plavsa, D., Clark, C., and Müller, R. D., 2017, A full-plate global reconstruction of the Neoproterozoic: Gondwana Research.

Milidragovic, D., and Francis, D., 2016, Ca. 2.7 Ga ferropicritic magmatism: A record of Fe-rich heterogeneities during Neoarchean global mantle melting: Geochimica et Cosmochimica Acta, no. 185, p. 44-63.

Mustard, P. S., 1991, Normal faulting and alluvial-fan deposition, basal Windermere Tectonic Assemblage, Yukon, Canada: Geological Society of America Bulletin, v. 103, no. 10, p. 1346-1364.

Mustard, P. S., and Roots, C. F., 1997, Rift-related volcanism, sedimentation, and tectonic setting of the Mount Harper Group, Ogilvie Mountains, Yukon Territory: Geological Survey of Canada Bulletin 492.

Pearce, J. A., 2008, Geochemical fingerprinting of oceanic basalts with applications to ophiolite classification and the search for Archean oceanic crust: Lithos, v. 100, no. 1-4, p. 14-48.

Pehrsson, S. J., and Buchan, K. L., 1999, Borden dykes of Baffin Island, Northwest Territories: a Franklin U-Pb baddeleyite age and a paleomagnetic reinterpretation: Canadian Journal of Earth Sciences, v. 36, no. 1, p. 65-73.

Rainbird, R. H., 1993, The Sedimentary Record of Mantle Plume Uplift Preceding Eruption of the Neoproterozoic Natkusiak Flood Basalt: The Journal of Geology, v. 101, no. 3, p. 305-318.

Rainbird, R. H., Jefferson, C. W., and Young, G. M., 1996, The early Neoproterozoic sedimentary Succession B of northwestern Laurentia: Correlations and paleogeographic significance: Geological Society of America Bulletin, v. 108, no. 4, p. 454-470.

Rapp, R. P., Shimizu, N., Norman, M. D., and Applegate, G. S., 1999, Reaction between slab-derived melts and peridotite in the mantle wedge: experimental constraints at 3.8 GPa: Chemical Geology, v. 160, no. 4, p. 335-356.

Rapp, R. P., and Watson, E. B., 1995, Dehydration Melting of Metabasalt at 8–32 kbar: Implications for Continental Growth and Crust-Mantle Recycling: Journal of Petrology, v. 36, no. 4, p. 891-931.

Rooney, A. D., Macdonald, F. A., Strauss, J. V., Dudas, F. O., Hallman, C., and Selby, D., 2014, Re-Os geochronology and coupled Os-Sr isotope constraints on the Sturtian snowball Earth: Proceedings of the National Academy of Science, v. 1073, p. 1-6.

Rooney, A. D., Strauss, J. V., Brandon, A. D., and Macdonald, F. A., 2015, A Cryogenian chronology: Two long-lasting synchronous Neoproterozoic glaciations: Geology, v. 43, no. 5, p. 459-462.

Shellnutt, J. G., Dostal, J., and Keppie, J. D., 2004, Petrogenesis of the 723 Ma Coronation sills, Amundsen basin, Arctic Canada: implications for the break-up of Rodinia: Precambrian Research, v. 129, no. 3–4, p. 309-324.

Smith, P. M., and Asimow, P. D., 2005, Adiabat_1ph: A new public front-end to the MELTS, pMELTS, and pHMELTS models: Geochemistry, Geophysics, Geosytems, v. 6, no. 1, p. 1-8.

Sobolev, A. V., Hofmann, A. W., Sobolev, S. V., and Nikogosian, I. K., 2005, An olivine-free mantle source of Hawaiian shield basalts: Nature, v. 434, no. 7033, p. 590-597.

Sobolev, S. V., Sobolev, A. V., Kuzmin, D. V., Krivolutskaya, N. A., Petrunin, A. G., Arndt, N. T., Radko, V. A., and Vasiliev, Y. R., 2011, Linking mantle plumes, large igneous provinces and environmental catastrophes: Nature, v. 477, no. 7364, p. 312-316.

Strauss, J. V., Macdonald, F. A., Halverson, G. P., Tosca, N., Schrag, D. P., and Knoll, A., 2015, Stratigraphic evolution of the Neoproterozoic Callison Lake Formation: Linking the break-up of Rodinia to the Islay carbon isotope excursion: American Journal of Science v. 315, p. 881-944.

Strauss, J. V., Macdonald, F. A., Taylor, J. F., Repetski, J. E., and McClelland, W. C., 2013, Laurentian origin for the North Slope of Alaska: Implications for the tectonic evolution of the Arctic: Lithosphere, v. 5, no. 5, p. 477-482.

Strauss, J. V., Rooney, A. D., Macdonald, F. A., Brandon, A. D., and Knoll, A. H., 2014, 740 Ma vase-shaped microfossils from Yukon, Canada: Implications for Neoproterozoic geochronology and biostratigraphy: Geology v. 42, p. 659–662.

Sun, S.-s., and McDonough, W. F., 1989, Chemical and isotopic systematics of oceanic basalts: implications for mantle composition and processes, *in* Saunders, A. D., and Norry, M. J., eds., Magmatism in the Ocean Basins: Geological Society, London, Special Publications 42, Volume 42, p. 313-345.

Taylor, S. R., and McLennan, S. M., 1995, The geochemical evolution of the continental crust: Rev. Geophys., v. 33, no. 2, p. 241-265.

Turner, S., and Hawkesworth, C., 1995, The nature of the sub-continental mantle: constraints from the major-element composition of continental flood basalts: Chemical Geology, v. 120, no. 3-4, p. 295-314.

Van Kooten, G. K., Watts, A. B., Coogan, J., Mount, V. S., Swenson, R. F., Daggett, P. H., Clough, J. G., Roberts, C. T., and Bergman, S. C., 1997, Geologic investigations of the Kandik Area, Alaska and adjacent Yukon Territory, Canada - RI96-6a: Alaska Division of Geological & Geophysical Surveys.

Wood, B. J., and Turner, S. P., 2009, Origin of primitive high-Mg andesite: Constraints from natural examples and experiments: Earth and Planetary Science Letters, v. 283, no. 1–4, p. 59-66.

Workman, R. K., and Hart, S. R., 2005, Major and trace element composition of the depleted MORB mantle (DMM): Earth and Planetary Science Letters, v. 231, no. 1–2, p. 53-72.

Young, G. M., 1982, The Late Proterozoic Tindir Group, east-central Alaska: Evolution of a continental margin: Geological Society of America Bulletin, v. 93, p. 759-783.

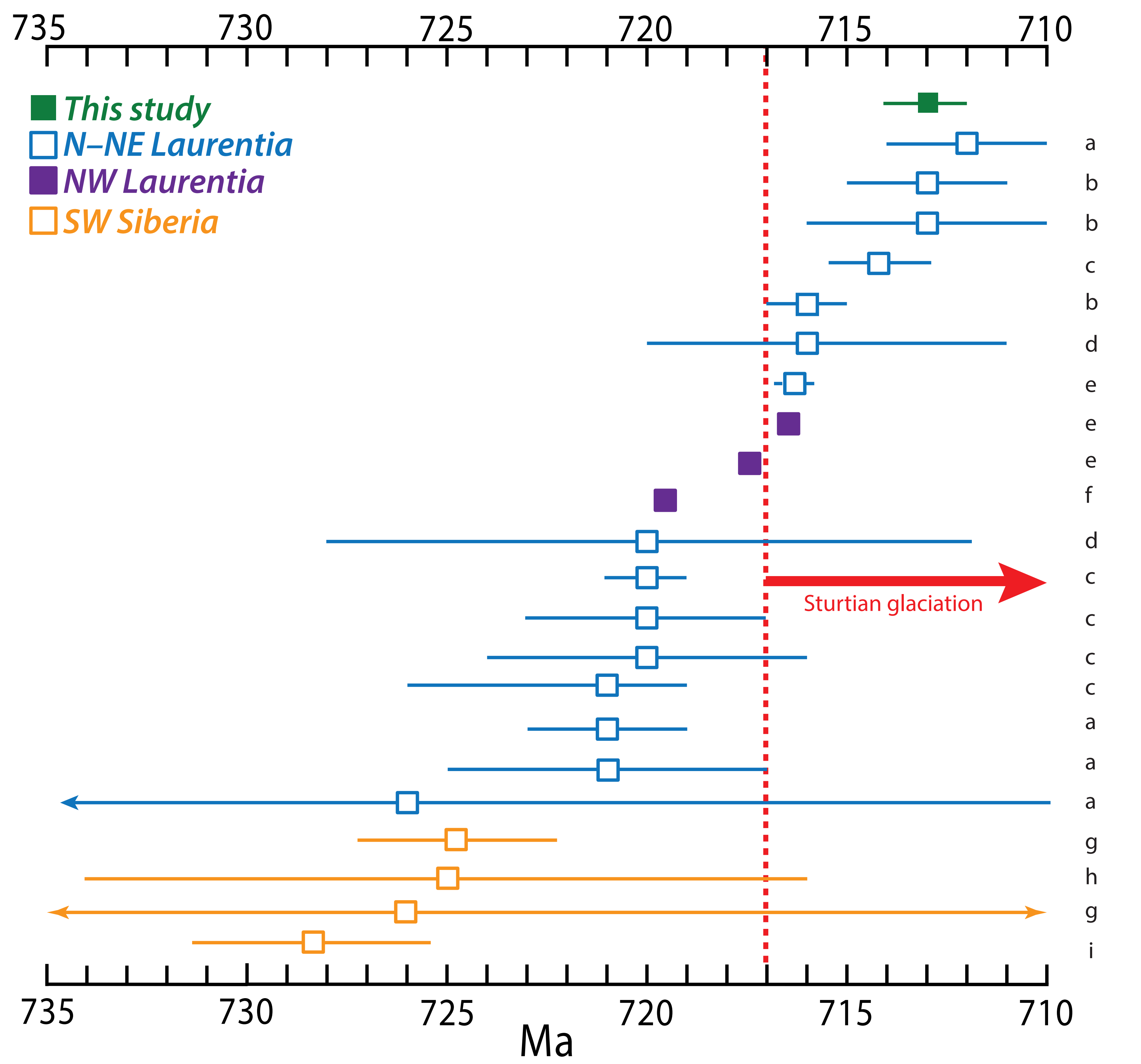

735
730
725
720
715
710
This study
N–NE Laurentia
NW Laurentia
SW Siberia
a
b
b
c
b
d
e
e
e
f
d
c
c
c
c
a
a
a
g
h
g
i
Sturtian glaciation
Ma

Greenland
Alaska
Canada
United States of America
1
2
1
3
4
5
6
7
7
8

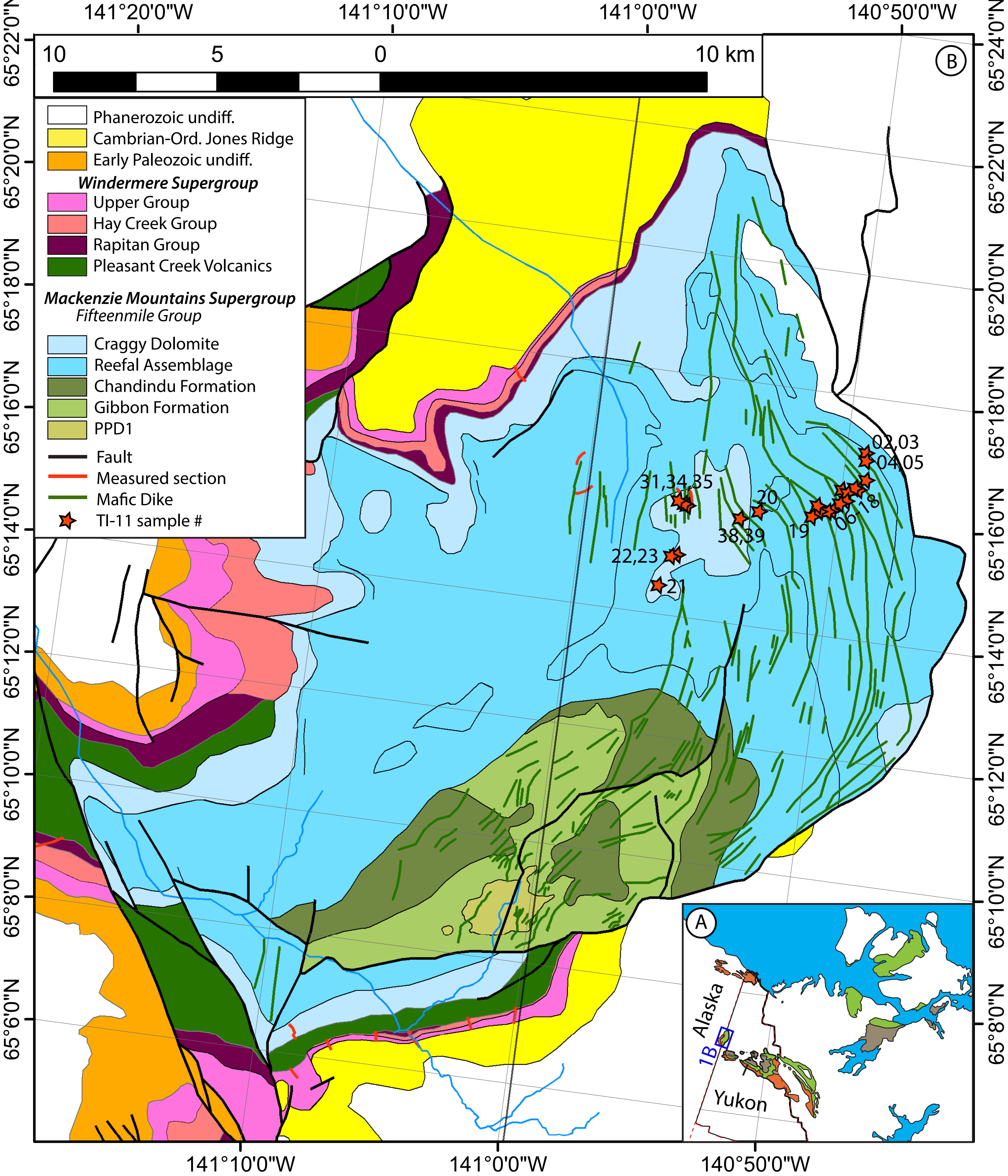

141°20'0"W
141°10'0"W
141°0'0"W
140°50'0"W
10
5
0
10 km
B
Phanerozoic undiff.
Cambrian-Ord. Jones Ridge
Early Paleozoic undiff.
Windermere Supergroup
Upper Group
Hay Creek Group
Rapitan Group
Pleasant Creek Volcanics
Mackenzie Mountains Supergroup
Fifteenmile Group
Craggy Dolomite
Reefal Assemblage
Chandindu Formation
Gibbon Formation
PPD1
Fault
Measured section
Mafic Dike
TI-11 sample #
02,03
04,05
31,34,35
20
38,39
19
06-18
22,23
21
A
Alaska
1B
Yukon
65°22'0"N
65°20'0"N
65°18'0"N
65°16'0"N
65°14'0"N
65°12'0"N
65°10'0"N
65°8'0"N
65°6'0"N
65°24'0"N

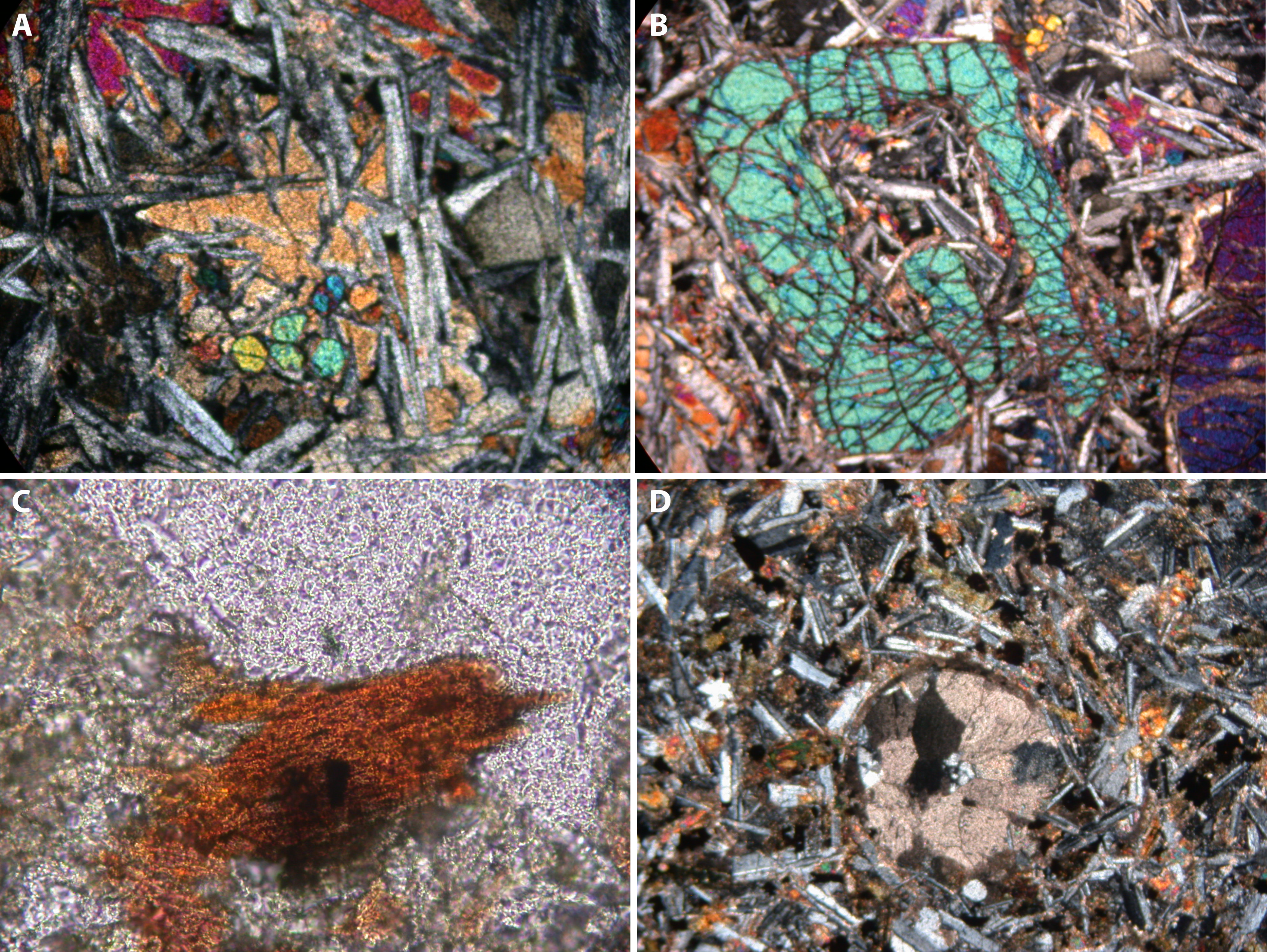
A
B
C
D

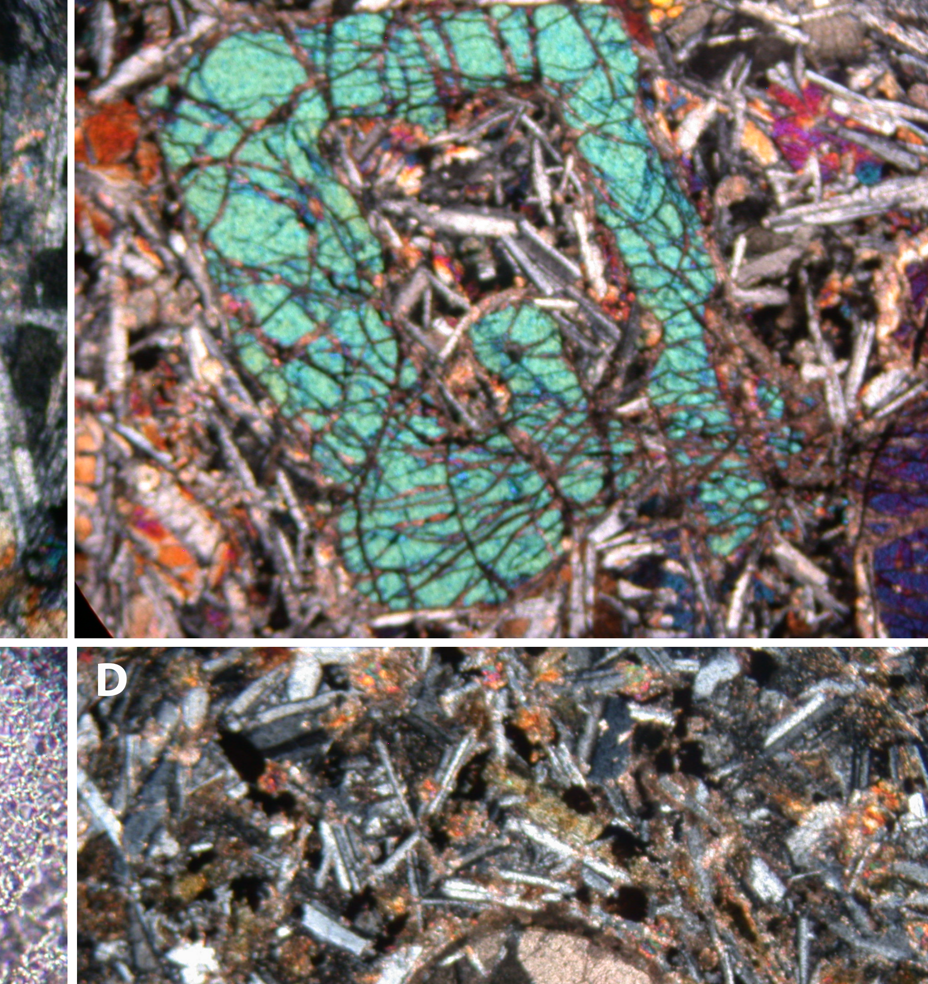
D

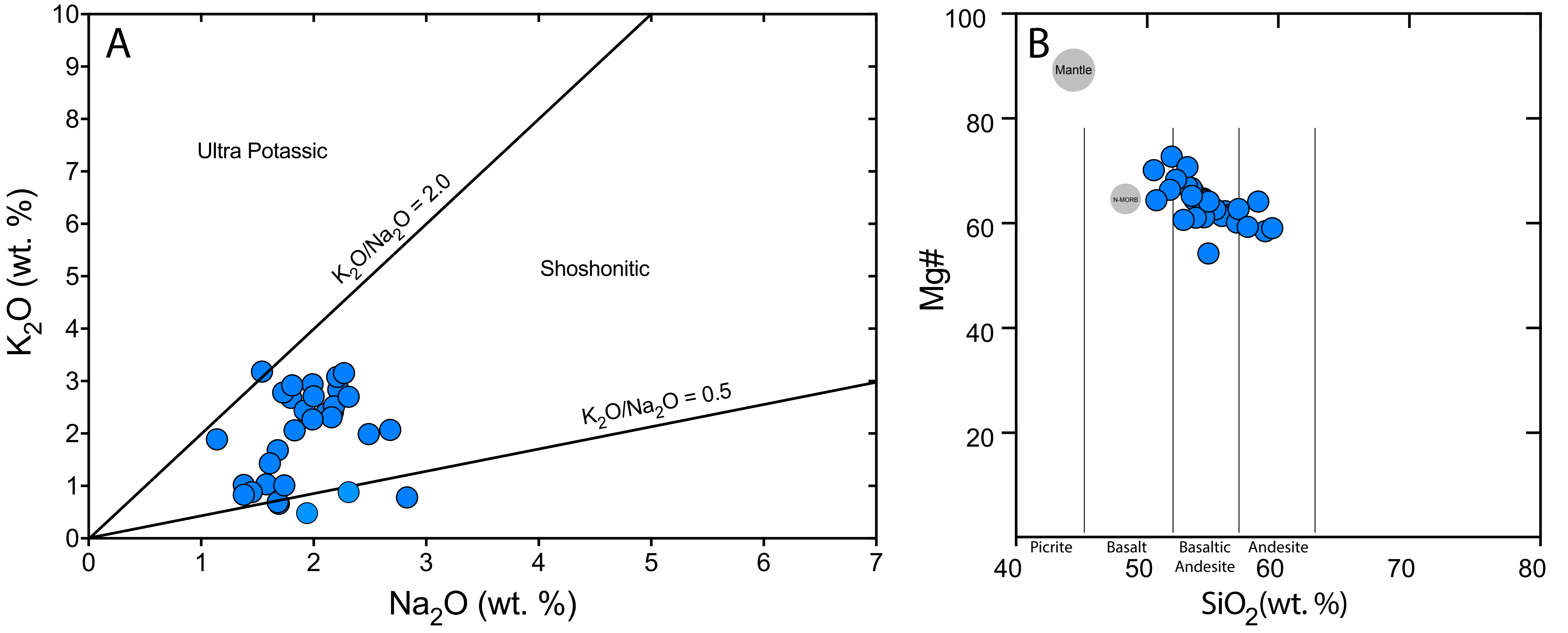
A
Ultra Potassic
Shoshonitic
K2O/Na2O = 2.0
K2O/Na2O = 0.5
K2O (wt. %)
Na2O (wt. %)
B
Mantle
N-MORB
Mg#
Picrite
Basalt
Basaltic Andesite
Andesite
SiO2(wt. %)

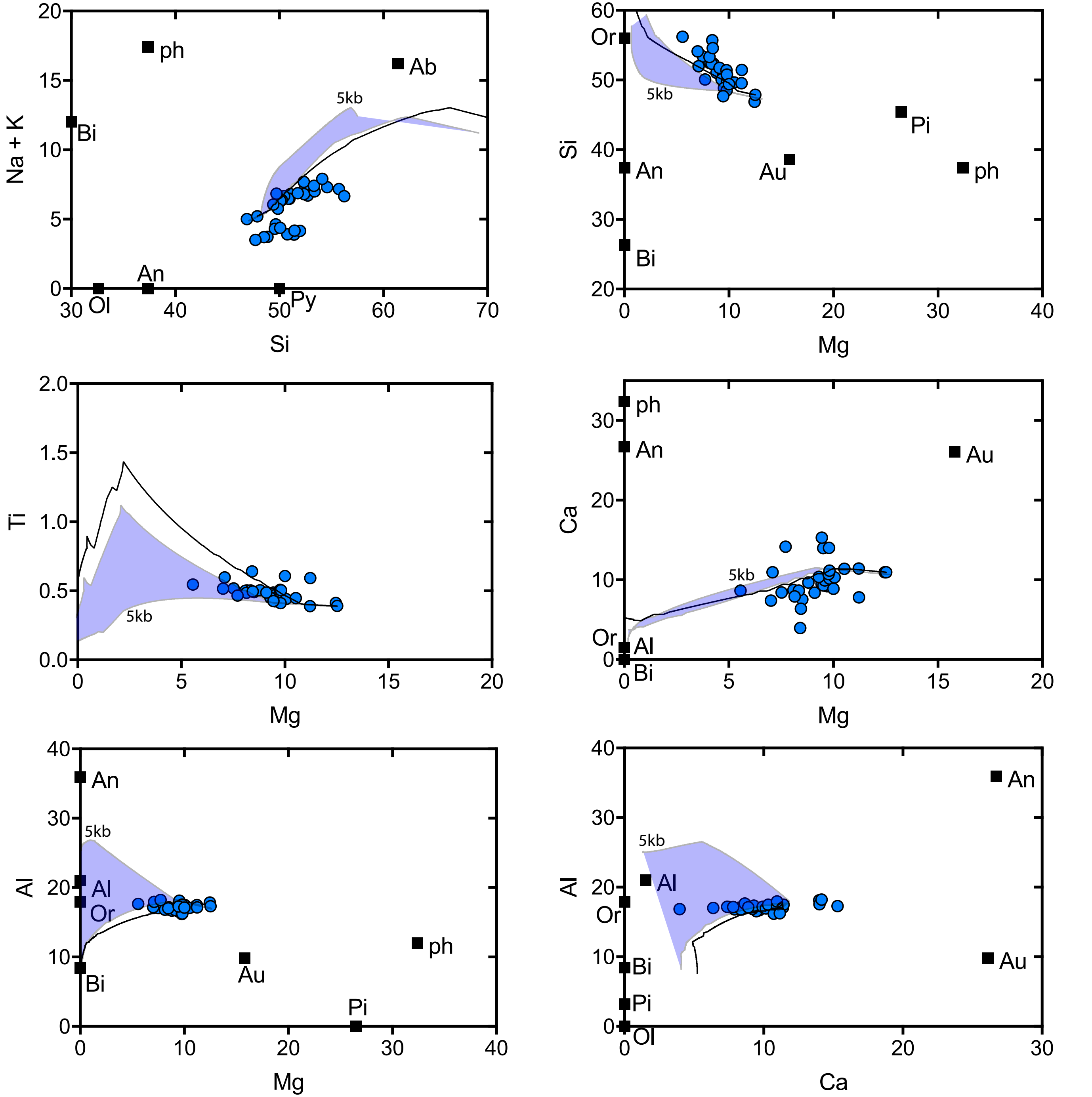

Na + K
Si
ph
Ab
Bi
5kb
An
Ol
Py
Si
Mg
Or
Pi
An
Au
ph
Bi
Ti
Mg
5kb
Ca
Mg
ph
An
Au
Or
Al
Bi
Al
Mg
An
5kb
Al
Or
Bi
Au
ph
Pi
Al
Ca
An
5kb
Al
Or
Bi
Pi
Ol
Au

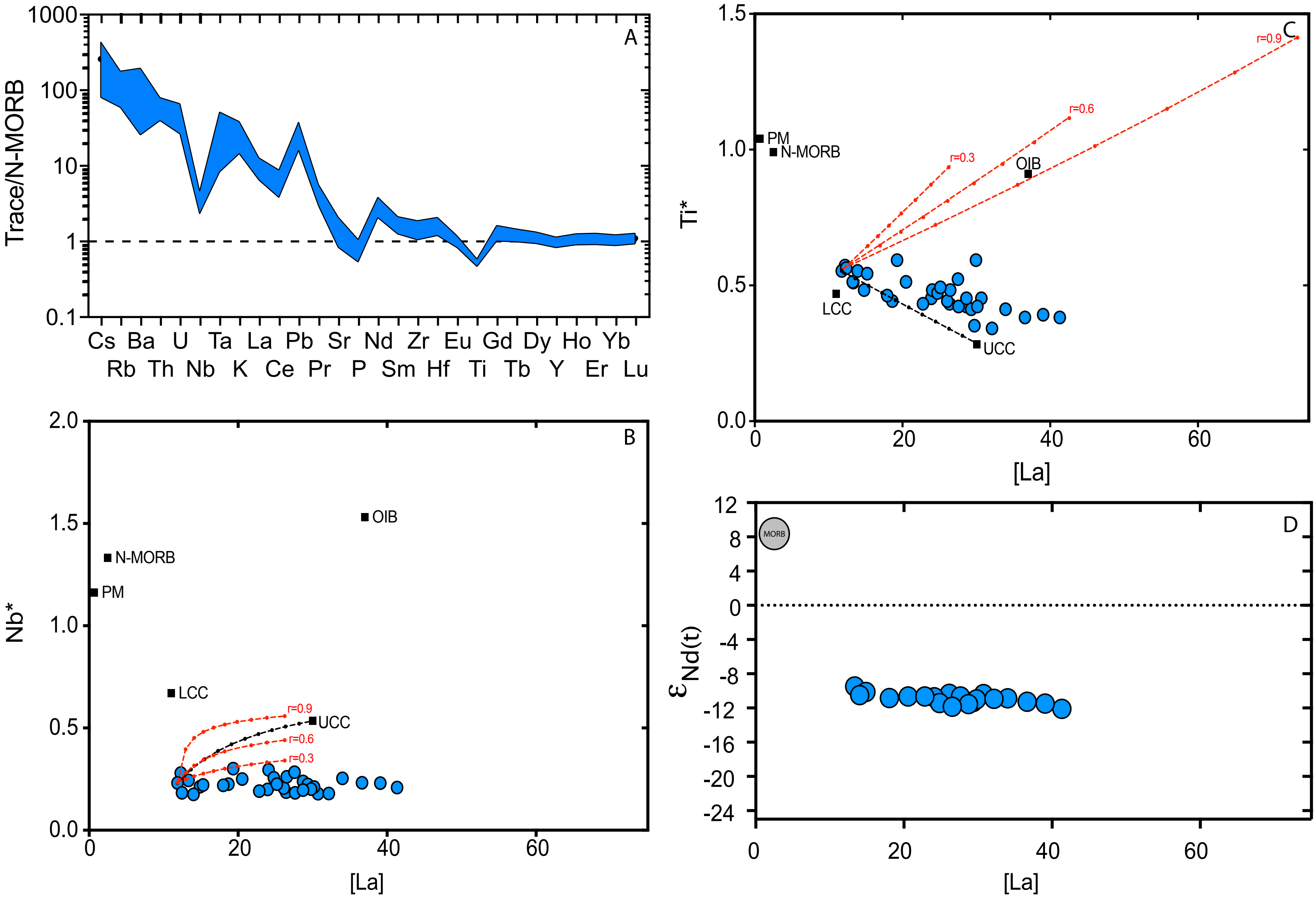

A
Trace/N-MORB
1000
100
10
1
0.1
Cs Ba U Ta La Pb Sr Nd Zr Eu Gd Dy Ho Yb
Rb Th Nb K Ce Pr P Sm Hf Ti Tb Y Er Lu
B
Nb*
[La]
OIB
N-MORB
PM
LCC
UCC
r=0.9
r=0.6
r=0.3
C
Ti*
[La]
PM
N-MORB
OIB
LCC
UCC
r=0.3
r=0.6
r=0.9
D
$\varepsilon_{Nd(t)}$
[La]
MORB

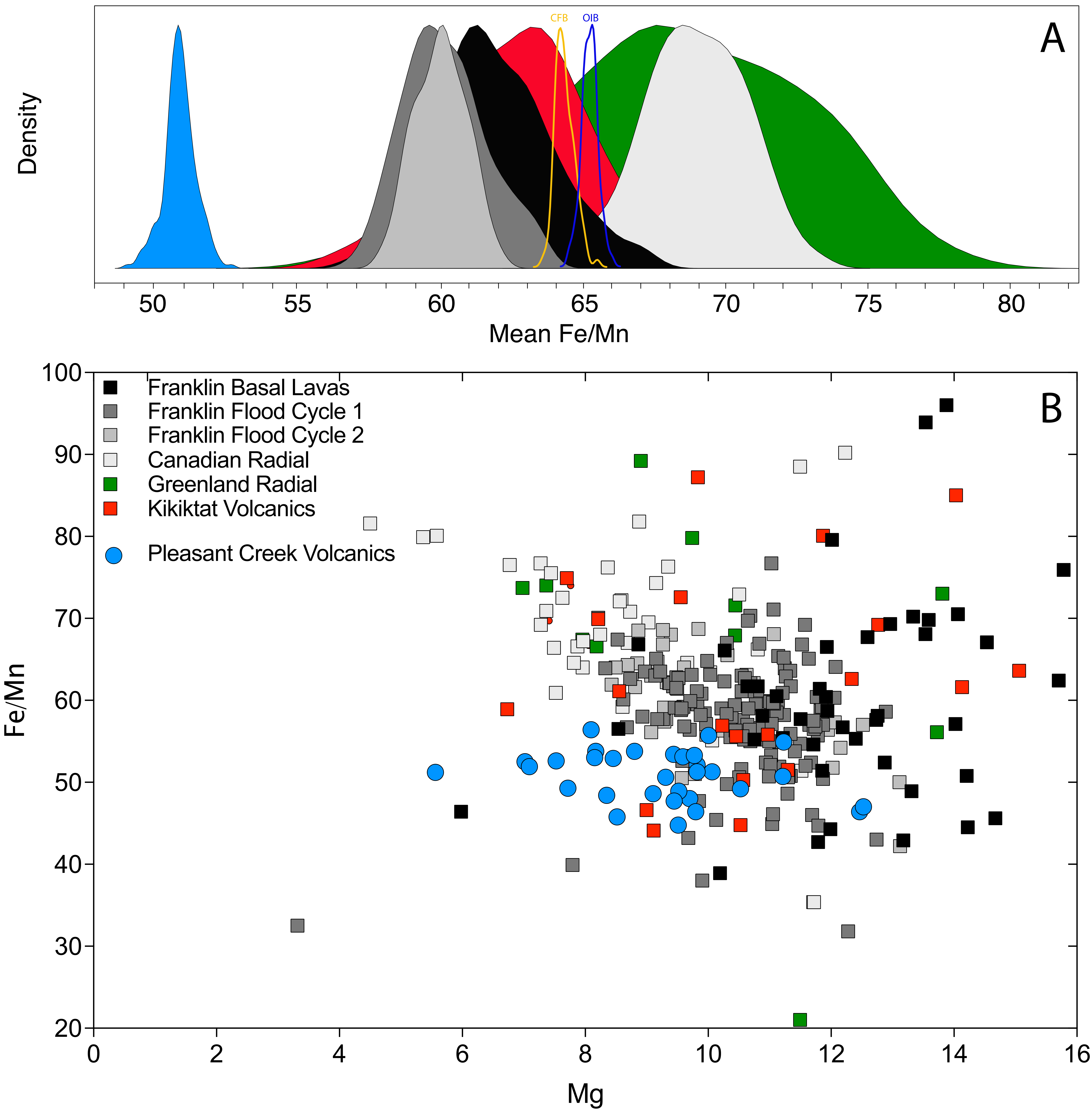

A
CFB
OIB
Density
50
55
60
65
70
75
80
Mean Fe/Mn
B
Franklin Basal Lavas
Franklin Flood Cycle 1
Franklin Flood Cycle 2
Canadian Radial
Greenland Radial
Kikiktat Volcanics
Pleasant Creek Volcanics
100
90
80
70
60
50
40
30
20
Fe/Mn
0
2
4
6
8
10
12
14
16
Mg

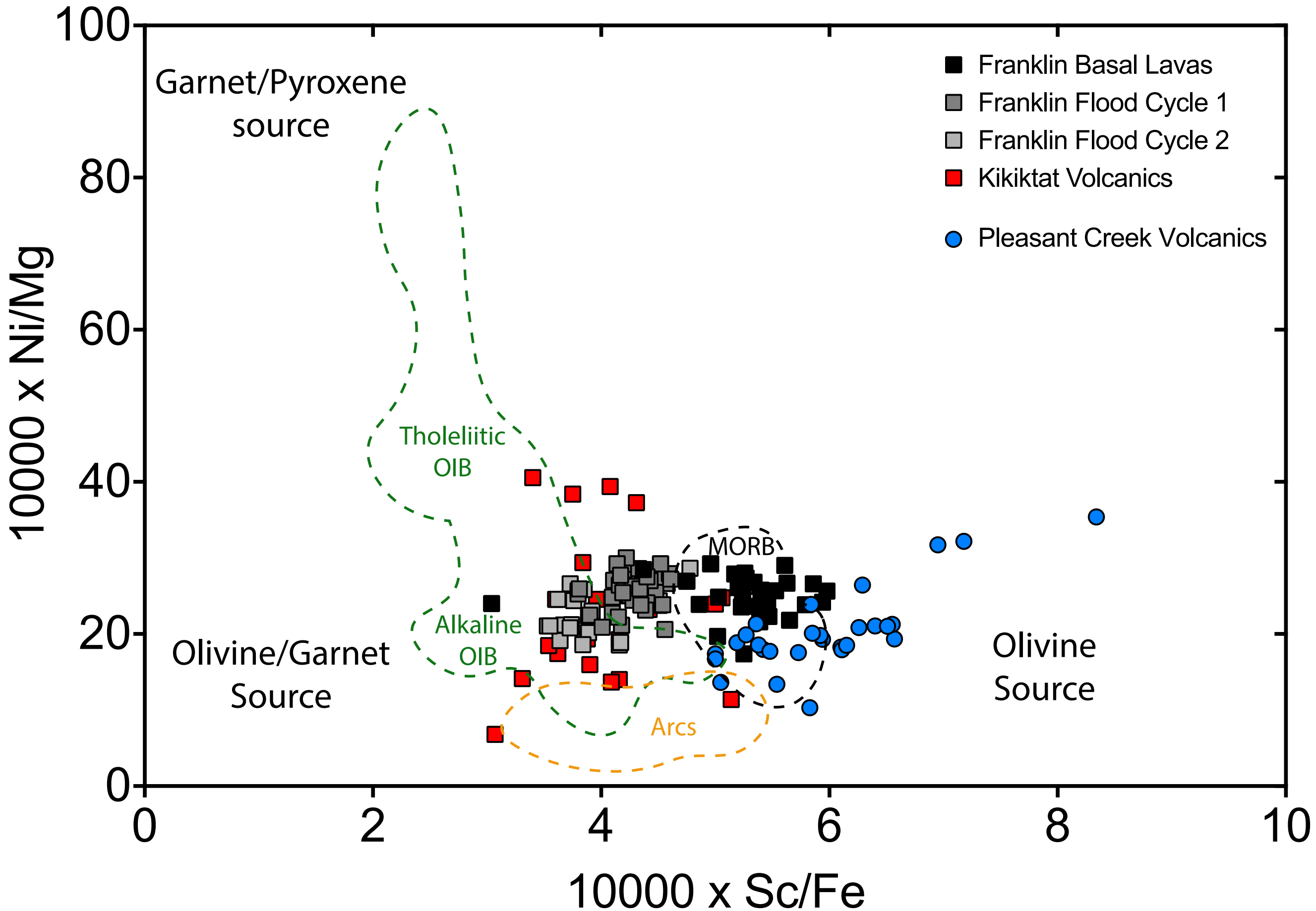

100
80
60
40
20
0
0
2
4
6
8
10
10000 x Ni/Mg
10000 x Sc/Fe
Garnet/Pyroxene
source
Tholeiitic
OIB
Alkaline
OIB
MORB
Arcs
Olivine/Garnet
Source
Olivine
Source
Franklin Basal Lavas
Franklin Flood Cycle 1
Franklin Flood Cycle 2
Kikiktat Volcanics
Pleasant Creek Volcanics

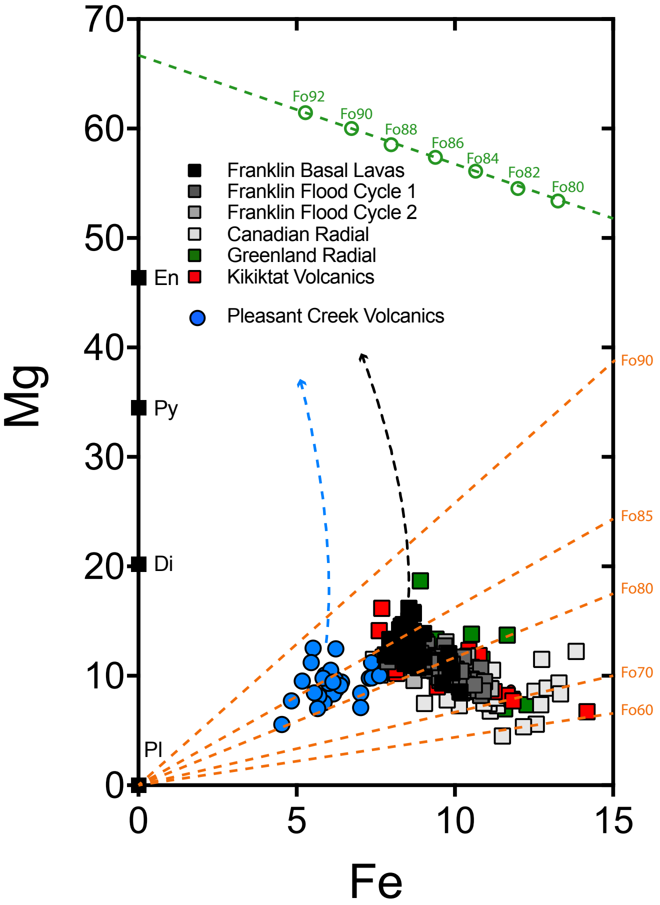

Mg
Fe
0
5
10
15
0
10
20
30
40
50
60
70
Fo92
Fo90
Fo88
Fo86
Fo84
Fo82
Fo80
Franklin Basal Lavas
Franklin Flood Cycle 1
Franklin Flood Cycle 2
Canadian Radial
Greenland Radial
Kikiktat Volcanics
Pleasant Creek Volcanics
En
Py
Di
Pl
Fo90
Fo85
Fo80
Fo70
Fo60

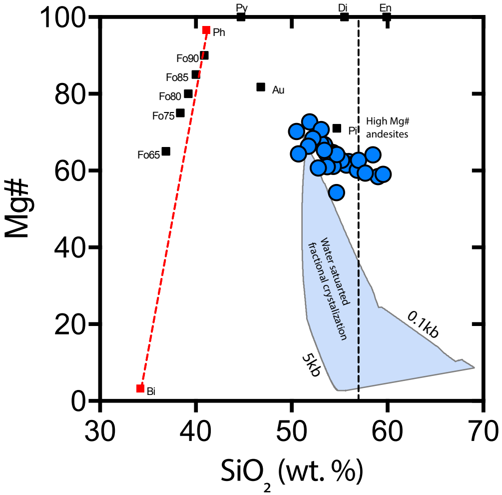

Py
Di
En
Ph
Fo90
Fo85
Fo80
Fo75
Fo65
Au
Pi
Bi
High Mg#
andesites
Water saturated
fractional crystalization
0.1kb
5kb
Mg#
0
20
40
60
80
100
30
40
50
60
70
SiO2 (wt. %)

Supplementary information for:

Cryogenian magmatism along the north-western margin of Laurentia: Plume or Rift?

Grant M. Cox[1,2*], Galen P. Halverson[3], Steven Denyszyn[4], John Foden[1], Francis A. Macdonald[5]

1. Centre for Tectonics Resources and Exploration (TRaX), Dept. of Earth Sciences, University of Adelaide, Adelaide, S.A.5005, Australia.
2. Curtin University, Dept. of Applied Geology, Bentley, WA, 6102, Australia.
3. Dept. Earth and Planetary Science, McGill University, Montréal, Québec, Canada.
4. School of Earth Sciences, University of Western Australia, Crawley, WA, 6009, Australia.
5. Dept. of Earth and Planetary Sciences, Harvard University, Cambridge, Massachusetts, U.S.A.

* Corresponding author: grant.cox@adelaide.edu.au

Sampling Methods

Sampling was conducted over 2 field seasons from traverses across the dykes and from measured sections for the lavas. The measured sections for the lavas is presented in Macdonald et al., (2011) and reproduced in Figure S1. Samples were chosen based on visual inspection with care taken to choose samples exhibiting the least amount of alteration, and specifically for the dykes, displaying no obvious signs of cumulate textures.

Figure S 1. Measured sections for the Pleasant Creek Volcanics.

Analytical Methods

U-Pb ID-TIMS Analysis:

Baddeleyite crystals were separated using the Wilfley water-shaking table in a technique modified after Söderlund & Johansson (2002). This method, using a pipette to remove a concentrate of small, dense, flat minerals off the Wilfley table, yielded several small baddeleyite grains. No pre-treatment methods were used beyond cleaning the grains with concentrated distilled HNO_3 and HCl and, due to their small size, no chemical separation methods were required. For ID-TIMS analysis, the samples were spiked with an in-house ^{205}Pb-^{235}U tracer solution, which has been calibrated against SRM981, SRM 982 (for Pb), and CRM 115 (for U), as well as an externally-calibrated U-Pb solution (the JMM solution from the EarthTime consortium). This tracer is regularly checked using "synthetic zircon" solutions that yield U-Pb ages of 500 Ma and 2000 Ma, provided by D. Condon (BGS).

Dissolution and equilibration of spiked single crystals was by vapour transfer of HF, using Teflon microcapsules in a Parr pressure vessel placed in a 200°C oven for six days. The resulting residue was re-dissolved in HCl and H_3PO_4 and placed on an outgassed, zone-refined rhenium single filament with 5µL of silicic acid gel. U–Pb isotope analyses were carried out using a Thermo Triton T1 mass spectrometer, in peak-jumping mode using a secondary electron multiplier. Uranium was measured as an oxide (UO_2). Fractionation and deadtime were monitored using SRM981 and SRM 982. Mass fractionation was 0.02 ± 0.07 %/amu. Data were reduced and plotted using the software packages Tripoli (from CIRDLES.org) and Isoplot (Ludwig, 2009). All uncertainties are reported at 2σ.

The weights of the baddeleyite crystals were calculated from measurements of photomicrographs and estimates of the third dimension. The weights are used to determine U concentration and do not contribute to the age calculation, and an uncertainty of 50% may be attributed to the concentration estimate.

XRF Analysis:

Rock samples were first trimmed to remove weathered surfaces and then cut into ~5 cm^3 fragments using a diamond-bladed rock saw. The rocks were crushed to rock chips in an iron jaw crusher. The chips where milled in a tungsten carbide mill until the powder could pass through a 75µm mesh. Major and trace element abundances were analyzed by X-ray fluorescence using a Philips PW2400 4kW automated XRF spectrometer system with a rhodium 60 kV end window X-ray tube. Major elements, Cr, Ni and V were analyzed using 32 mm diameter fused beads prepared from a 1:5 sample/lithium tetraborate mixture. Sc, Rb, Sr, Zr, Nb and Y were analyzed using 40mm diameter pressed pellets prepared at a pressure of 20 tons from a mixture of 10g sample powder with 2g Hoechst Wax C Micropowder. Calibration regression lines were prepared using between 15 and 40 International Standard Reference Materials. Corrections for mass absorption effects were applied on concentration values using a combination of alpha coefficients and/or Compton scatter. The accuracy for silica is within 0.5% absolute, and is within 1% for other majors and within 5% for trace elements. Instrument precision is within 0.3% relative, generally within 0.23% relative, and the overall precision for beads and pressed pellets is within 0.5% relative. Results can be found in the electronic supplementary material.

Trace Element Analysis:

Rock samples were first trimmed to remove weathered surfaces and then cut into ~5 cm^3 fragments using a diamond-bladed rock saw. The rocks were crushed to rock chips in an iron jaw crusher. The chips where milled in a tungsten carbide mill until the powder could pass through a 75µm mesh. The resulting powder was weighed (~0.02g) into cleaned teflon bombs and dissolved under pressure with a HF-HNO_3 mixture. The resulting solutions were evaporated and dissolved again in perchloric acid to facilitate conversion of fluoride salts to chloride salts. The samples were then dissolved in aqua-regia followed by 6N HCl then finally in 6N HNO_3. The resulting material was redissolved in 5% HNO_3 and analysised for trace elements on a Perkins Elmer quadruple ICP-MS. Results can be found in the supplementary material.

Sm-Nd ID-TIMS Analysis

Sm and Nd concentrations were determined by isotope dilution. Approximately ~ 0.3g of sample powder was spiked with enriched ^{150}Nd-^{149}Sm tracers and dissolved under pressure with a HF-HNO_3 mixture in Teflon containers. The resulting solutions were evaporated and dissolved again in perchloric acid to facilitate conversion of fluoride salts to chloride salts. The samples were then dissolved in aqua-regia followed by 6N HCl. Nd and Sm were extracted using a three stage-chemistry procedure. The first stage involved the removal of Fe by passing the sample through columns filled with 200-400 mesh AG1X8 anion exchange resin. Subsequent to the removal of Fe, the REE component was concentrated using columns filled with Eichrom TRU Resin SPS 50-100µm. The third stage purification of the Sm and Nd fractions entailed passing the samples through columns filled with 600 mg of Eichrom LN Resin 100-150µm.

The ^{143}Nd/^{144}Nd and ^{147}Sm/^{144}Nd ratios reported were measured on a Thermo Triton mass spectrometer in the GEOTOP laboratories at Université du Québec à Montréal. Nd and Sm were analyzed using a double filament array with the samples loaded onto outgassed Re filaments, parallel to this was an outgassed Re ionization filament. Nd and Sm samples were measured in dynamic mode, the total combined blank for Sm and Nd is less than 150 pg. The reported Sm and Nd concentrations and the ^{147}Sm/^{144}Nd ratios have less than 0.5% error, corresponding to an error of less than 0.5 ε_{Nd} unit for the initial Nd isotopic composition. ^{146}Nd/^{144}Nd was normalized to 0.7219 for mass fractionation corrections. Repeated measurements of JNdi-1 standard yielded a value of ^{143}Nd/^{144}Nd = 512109 ± 1 (n =20) for the period of the study. This value is within error of the value obtained by Tanaka et al. (2000) of ^{143}Nd/^{144}Nd = 0.512115 ± 7. Repeated measurements of BHVO-2 yielded a value of ^{143}Nd/^{144}Nd = 0.512965 ± 6 (n = 20) for the period of the study. This value is within error of the accepted value of ^{143}Nd/^{144}Nd = 0.51298 ± 12 (Jochum et al., 2005). The chondritic reference values used for ε_{Nd} calculations are; ^{143}Nd/^{144}Nd$_{CHUR}$ = 0.512636, ^{147}Sm/^{144}Nd$_{CHUR}$ = 0.1966, and the decay constant for ^{147}Sm was assumed to be 6.54 x 10^{-12} a^{-1}.

References

Jochum, K.P., Nohl, U., Herwig, K., Lammel, E., Stoll, B., Hofmann, A.W., 2005. GeoReM: A New Geochemical Database for Reference Materials and Isotopic Standards. Geostandards and Geoanalytical Research 29, 333-338.

Ludwig, K.R., 2009. Isoplot Ver:3.0.

Macdonald, F.A., Smith, E.F., Strauss, J.V., Cox, G.M., Halverson, G.P., Roots, C.F., 2011. Neoproterozoic and early Paleozoic correlations in the western Ogilvie Mountains, in: MacFarlane, K.E., Weston, L.H., Blackburn, L.R. (Eds.), Yukon Exploration and Geology, pp. 161-182.

Söderlund, U., Johansson, L., 2002. A simple way to extract baddeleyite (ZrO2). Geochemistry Geophysics Geosystems 3.

Tanaka, T., Togashi, S., Kamioka, H., Amakawa, H., Kagami, H., Hamamoto, T., Yuhara, M., Orihashi, Y., Yoneda, S., Shimizu, H., Kunimaru, T., Takahashi, K., Yanagi, T., Nakano, T., Fujimaki, H., Shinjo, R., Asahara, Y., Tanimizu, M., Dragusanu, C., 2000. JNdi-1: a neodymium isotopic reference in consistency with LaJolla neodymium. Chemical Geology 168, 279-281.

Table S1: U-Pb isotopic data for baddeleyites from the Tatonduk dyke (TI10-010; 65.14021 N, 141.00488 W).

Sample	wt. (µg)	U (ppm)	Pb_c (pg)	mol% Pb*	$\frac{Th}{U}$	$\frac{^{206}Pb}{^{204}Pb}$	$\frac{^{207}Pb}{^{206}Pb}$	± (%)	$\frac{^{207}Pb}{^{235}U}$	± (%)	$\frac{^{206}Pb}{^{238}U}$	± (%)	ρ	$^{206}Pb/^{238}U$ Age (Ma)	± (Ma)	$^{207}Pb/^{206}Pb$ Age (Ma)	± (Ma)
1	0.1	49	0.3	83	0.04	266	0.06338	0.8	1.0233	0.88	0.11711	0.15	0.56	713.9	1.1	720.9	17.1
2	0.2	436	3.1	61	0.03	120	0.06217	5.14	1.0027	5.55	0.11697	0.42	0.99	713.1	3	680	109.8
3	0.1	100	2	40	0.04	54	0.06142	7.88	0.9906	8.5	0.11696	0.65	0.96	713	4.6	654	169
4	0.3	250	1.1	89	0.21	475	0.06368	5.49	1.0276	5.94	0.11704	0.46	0.99	713.5	3.3	730.9	116.3
5	0.1	96	1.2	47	0.04	74	0.06236	5.52	0.9947	5.96	0.11568	0.49	0.92	705.7	3.4	686.5	117.8

Sample weights are calculated from crystal dimensions and are associated with an arbitrary 50% uncertainty.

Pb_c = Total common Pb including analytical blank (0.8±0.3 pg per analysis). Blank composition is: $^{206}Pb/^{204}Pb = 18.55 \pm 0.63$, $^{207}Pb/^{204}Pb = 15.50 \pm 0.55$, $^{208}Pb/^{204}Pb = 38.07 \pm 1.56$ (all 2σ), and a $^{206}Pb/^{204}Pb$ – $^{207}Pb/^{204}Pb$ correlation of 0.9.

Th/U calculated from radiogenic $^{208}Pb/^{206}Pb$ and age.

Measured isotopic ratios corrected for tracer contribution and mass fractionation (0.02 ± 0.07 %/amu).

ρ = error correlation coefficient of radiogenic $^{207}Pb/^{235}U$ vs. $^{206}Pb/^{238}U$.

All uncertainties given at 2σ

Table S2. Major and trace element analysis.

Sample Name	TI10-011	TI10-012	TI10-013	TI10-023	TI10-025	TI10-026	TI10-028	TI10-029	TI10-030	TI11-002
Lat (N):	65.14031	65.13871	65.13871	65.14956	65.14956	65.15316	65.15453	65.15280	65.15276	65.28332
Long (W):	141.00674	140.99735	140.99735	140.98102	140.98102	140.97981	140.97602	140.97800	140.97800	140.82280
Rock Type:	Dyke	Dyke	Dyke	Dyke	Dyke	Dyke	Dyke	Dyke	Dyke	Dyke
Major element analysist (wt. %):										
SiO2	57.1	54.5	54.4	53.4	53.2	54.7	53.6	54.3	55.4	52.9
TiO2	0.9	0.7	0.7	0.7	0.7	0.7	0.7	0.7	0.7	0.7
Al2O3	14.6	15.0	15.1	14.8	14.7	15.0	15.1	14.9	15.0	15.4
Fe2O3T	9.6	8.2	8.4	8.7	8.9	8.2	8.7	8.5	8.1	8.5
MnO	0.1	0.1	0.2	0.1	0.1	0.1	0.2	0.2	0.1	0.2
MgO	5.8	5.7	5.9	6.2	6.6	5.6	6.9	5.8	5.2	6.7
CaO	3.8	8.0	7.3	9.5	9.2	8.5	9.0	8.4	8.2	9.1
Na2O	1.9	2.2	2.2	2.1	1.8	2.1	1.7	1.8	2.1	2.1
K2O	2.8	2.8	3.0	2.4	2.6	2.3	2.7	2.9	2.5	2.3
P2O5	0.2	0.1	0.1	0.1	0.1	0.1	0.1	0.1	0.1	0.1
LOI	3.6	2.7	3.0	2.1	2.2	2.7	1.7	2.4	2.5	2.3
Total	100.3	100.0	100.1	100.2	100.1	100.0	100.3	99.9	100.0	100.2
Trace element analysis (ppm):										
Ni	36	66	70	67	77	62	80	65	56	71
Cr2O3	130.7	416	446.9	344.2	435.9	404.2	448.8	414.2	345.9	452.5
Co	24	23	23	20	25	22	30	26	24	31
Sc	39	27	28	33	37	35	40	32	31	34
V	178.9	168	167.7	181	186	165.4	187.9	168.8	159	180.9
Ga	17.4	16.14	15.6	15.3	15.425	16.3	15.6	15.8	16.8	15.33
Cu	96	46	53	35	50	39	52	40	48	60
Zn	51	31	126	37	33	35	44	69	46	54
Cs	5.1	1.3	1.3	1.0	1.3	1.2	2.1	1.5	1.2	1.1
Rb	98.5	98.4	99.9	90.9	106.6	84.1	97.5	120.6	95.5	90.4
Ba	575.7	641.5	870.3	921.8	1220.1	432.9	515.3	749.1	577.7	429.7
Th	11.1	7.7	7.7	6.3	6.6	8.3	5.6	6.9	9.5	8.4
U	5.6	2.3	2.4	3.0	2.5	4.0	2.7	2.8	2.2	2.6
Nb	16.2	9.9	9.6	8.5	8.5	10.1	8.2	9.9	11.2	8.0
Ta	1.4	1.0	2.0	0.8	0.8	0.9	1.1	1.1	1.4	6.9
La	41.3	28.7	29.4	26.5	26.1	30.7	24.0	30.2	34.0	27.7
Ce	83.0	53.0	55.0	37.0	54.0	74.0	62.0	72.0	78.0	79.0
Pb	13.3	7.5	12.3	6.1	7.1	9.5	9.3	13.4	12.8	10.3
Pr	9.6	6.8	6.9	6.2	6.1	7.1	5.6	6.8	7.8	6.6
Mo	2.0	1.0	0.6	1.7	0.4	0.6	2.0	0.9	1.2	0.8
Sr	77.6	97.4	96.9	116.9	121.7	101.5	114.1	99.1	102.2	120.8
P	712.9	516.1	507.7	485.3	463.4	520.2	451.5	505.8	555.1	450.2
Nd	35.7	25.7	25.7	23.2	22.7	26.4	21.1	25.7	29.1	24.9
Sm	7.1	5.3	5.3	4.8	4.7	5.3	4.4	5.3	5.8	5.1
Zr	200.6	129.5	127.0	115.7	114.4	133.1	109.9	127.9	142.3	108.1
Hf	5.6	3.8	3.6	3.4	3.4	3.7	3.1	3.7	4.1	3.9
Eu	1.6	1.1	1.1	1.1	1.2	1.0	1.0	1.1	1.1	1.1
Gd	8.2	5.9	6.1	5.7	5.0	5.4	5.2	6.0	6.5	5.4
Tb	1.2	0.9	0.9	0.9	0.8	0.9	0.8	0.9	1.0	1.0
Dy	7.7	5.4	5.4	5.4	5.2	5.4	5.1	5.5	5.8	6.1
Y	44.1	29.9	29.5	29.7	29.1	29.8	27.8	29.9	31.4	28.3
Ho	1.6	1.1	1.1	1.1	1.1	1.1	1.1	1.2	1.2	1.3
Er	4.9	3.3	3.4	3.4	3.3	3.3	3.2	3.4	3.6	3.8
Yb	4.9	3.4	3.4	3.4	3.4	3.4	3.3	3.5	3.6	3.7
Lu	0.7	0.5	0.5	0.5	0.5	0.5	0.5	0.5	0.5	0.6

Sample Name	TI11-003	TI11-005	TI11-006	TI11-007	TI11-008	TI11-009	TI11-010	TI11-014	TI11-016	TI11-017	TI11-018
Lat (N):	65.28332	65.2812	65.27573	65.27299	65.27262	65.27151	65.27191	65.26677	65.26591	65.26517	65.2628
Long (W):	140.82280	140.82185	140.82049	140.82588	140.82814	140.83077	140.83428	140.84224	140.85027	140.85243	140.85866
Rock Type:	Dyke	Dyke	Dyke	Dyke	Dyke	Dyke	Dyke	Dyke	Dyke	Dyke	Dyke
Major element analysist (wt. %):											
SiO2	52.7	52.4	52.5	49.4	55.8	52.6	54.2	52.4	57.2	51.1	56.6
TiO2	0.6	0.6	0.7	0.6	0.7	0.6	0.7	0.6	0.7	0.6	0.7
Al2O3	15.3	15.3	15.2	16.0	14.9	15.6	14.9	15.3	15.1	15.7	15.2
Fe2O3T	8.4	8.4	8.2	8.7	7.9	8.3	8.9	8.5	7.7	7.8	7.9
MnO	0.1	0.1	0.1	0.2	0.1	0.1	0.2	0.2	0.1	0.1	0.1
MgO	6.8	6.5	7.0	8.8	5.7	7.1	6.4	7.5	5.9	9.0	4.9
CaO	9.7	10.1	10.0	10.8	7.7	10.2	8.2	11.2	6.2	10.9	7.2
Na2O	1.9	2.0	2.4	1.6	2.3	1.8	2.0	1.6	2.6	2.3	2.2
K2O	2.4	2.2	2.0	1.6	2.6	2.0	2.7	1.4	2.0	0.9	3.1
P2O5	0.1	0.1	0.1	0.1	0.1	0.1	0.1	0.1	0.1	0.1	0.1
LOI	2.2	2.3	2.4	2.5	2.3	1.8	2.2	1.7	2.4	2.1	2.0
Total	100.2	100.0	100.5	100.3	100.2	100.2	100.3	100.4	100.2	100.5	100.1
Trace element analysis (ppm):											
Ni	73	73	83	113	47	81	67	96	48	129	59
Cr2O3	480.6	478.5	500.8	558.4	376.8	517.5	387	342	412.4	631.3	323.4
Co	30	31	35	44	32	39	39	39	36	48	31
Sc	36	36	34	40	28	30	31	32	30	32	29
V	180.1	178.1	170.8	185.2	155.1	165.1	167.2	179.2	141.8	182.1	147.6
Ga	15.39	14.99	15.16	14.46	15.73	15.89	15.77	15.33	15.52	13.9	15.96
Cu	57	55	81	65	44	61	68	81	48	75	51
Zn	61	50	62	49	62	89	82	49	54	67	55
Cs	1.0	0.6	0.6	0.9	1.3	1.0	1.1	1.2	1.2	0.8	1.8
Rb	98.0	81.3	62.8	53.6	94.1	71.4	98.5	48.5	63.3	29.6	107.0
Ba	466.2	415.8	437.0	370.5	500.0	450.4	645.1	384.8	1538.2	788.2	1170.1
Th	7.8	7.8	9.0	4.7	10.4	8.1	8.2	7.1	10.7	4.4	11.8
U	1.7	1.8	1.3	1.0	3.5	2.4	1.5	2.2	2.3	1.3	2.6
Nb	7.4	7.7	8.5	4.6	10.1	8.0	8.0	7.0	10.4	4.8	11.5
Ta	6.5	5.4	23.3	3.1	7.4	9.0	5.6	5.2	6.8	5.9	8.4
La	29.8	20.6	24.1	13.4	28.7	32.2	24.8	22.8	26.5	14.9	36.6
Ce	75.0	72.0	69.0	63.0	38.0	32.0	31.0	21.0	23.0	30.5	32.0
Pb	6.9	8.3	8.7	4.4	10.4	9.1	11.6	8.1	12.1	11.3	12.8
Pr	7.1	5.0	5.8	3.3	6.8	7.7	5.9	5.5	6.3	3.6	8.6
Mo	1.7	0.5	0.7	0.5	0.7	0.8	0.8	0.7	0.8	0.5	0.8
Sr	133.0	133.1	183.2	151.5	164.3	136.0	168.7	91.6	242.6	143.3	365.0
P	436.1	433.0	444.8	325.8	508.1	421.1	467.1	410.9	526.5	328.3	556.2
Nd	27.0	19.1	22.0	13.1	25.7	28.6	22.3	21.1	23.5	14.0	32.0
Sm	5.6	3.9	4.4	3.0	5.0	5.8	4.5	4.4	4.6	3.1	6.3
Zr	100.5	102.1	111.1	66.7	133.7	106.9	114.7	96.1	142.7	71.3	148.3
Hf	4.2	3.1	3.7	2.3	4.0	4.4	3.7	3.5	3.7	2.4	5.0
Eu	1.3	0.9	1.0	0.9	1.0	1.3	1.0	1.1	1.1	0.9	1.3
Gd	5.9	4.1	4.5	3.5	5.2	5.9	4.8	4.8	4.7	3.5	6.3
Tb	1.1	0.7	0.8	0.7	0.9	1.0	0.9	0.9	0.8	0.7	1.1
Dy	6.8	4.7	5.1	4.5	5.5	6.6	5.4	5.6	4.9	4.3	6.6
Y	26.8	27.1	26.8	23.0	29.6	25.9	29.0	25.7	32.2	23.2	32.5
Ho	1.4	1.0	1.1	1.0	1.2	1.4	1.1	1.2	1.0	0.9	1.4
Er	4.3	3.0	3.1	3.0	3.4	4.1	3.3	3.5	3.1	2.8	4.0
Yb	4.1	2.8	3.0	2.9	3.2	3.9	3.2	3.4	2.8	2.7	3.8
Lu	0.7	0.4	0.5	0.5	0.5	0.6	0.5	0.5	0.5	0.4	0.6

Sample Name	TI11-030	TI11-037	TI11-038	TI11-041	TI10-001	TI10-002	TI10-006	TI10-007	TI10-017	TI10-018	TI10-019
Lat (N):	65.26271	65.26163	65.26163	65.26283	65.12349	65.12191	65.11706	65.11923	65.11527	65.11500	65.11549
Long (W):	140.9411	140.9005	140.9005	140.94127	141.01268	141.00890	141.02245	141.02002	141.03535	141.03525	141.04462
Rock Type:	Dyke	Dyke	Dyke	Dyke	Lava	Lava	Lava	Lava	Lava	Lava	Lava
Major element analysist (wt. %):											
SiO2	53.1	57.6	51.9	52.3	50.9	51.3	49.6	49.8	50.8	49.1	50.3
TiO2	0.7	0.7	0.5	0.7	0.8	0.8	0.6	0.6	0.6	0.6	0.8
Al2O3	14.2	15.3	15.5	14.2	14.9	14.5	15.6	15.3	15.7	15.1	14.8
Fe2O3T	10.0	6.2	7.6	10.1	9.2	9.8	7.0	8.0	6.5	8.4	10.3
MnO	0.2	0.1	0.1	0.2	0.2	0.2	0.1	0.2	0.1	0.2	0.2
MgO	6.8	3.8	7.9	6.8	4.7	7.5	6.5	6.8	5.3	6.5	6.8
CaO	10.3	8.3	11.2	10.7	10.0	7.3	13.3	13.4	13.4	14.7	8.4
Na2O	1.7	1.5	1.1	1.6	1.5	1.8	1.3	1.4	1.7	1.3	2.7
K2O	0.6	3.1	1.9	0.7	1.0	0.5	1.0	0.9	1.0	0.8	0.7
P2O5	0.1	0.1	0.1	0.1	0.1	0.1	0.1	0.1	0.1	0.1	0.2
LOI	2.8	3.6	2.7	2.6	6.5	5.9	4.8	3.6	4.8	3.5	4.8
Total	100.4	100.2	100.4	100.1	99.6	99.6	99.9	100.0	99.9	100.2	100.0
Trace element analysis (ppm):											
Ni	82	48	100	86	47	104	124	131	112	104	126
Cr2O3	331.9	333.9	632	343.5	217.4	507.2	675.5	711.1	582.4	572.1	552.6
Co	43	26	40	49	27	31	31	36	34	32	41
Sc	41	27	34	46	32	31	34	40	38	37	29
V	202.1	145.1	169.9	220.1	215.8	181.2	194.4	204.5	199.5	201.9	186.8
Ga	14.2	17.2	14.1	14.0	15.7	16.4	13.9	13.8	14.2	14.3	16.4
Cu	172	43	63	183	62	68	69	61	73	71	79
Zn	49	69	43	51	52	54	43	40	39	38	56
Cs	5.9	4.3	1.6	13.0	0.6	1.1	1.3	0.7	0.4	0.9	0.8
Rb	17.5	113.9	48.5	18.0	31.4	18.5	25.7	29.5	24.8	32.3	24.3
Ba	2772.8	762.4	652.6	2075.3	639.5	413.7	295.1	212.3	267.9	160.6	420.0
Th	5.8	13.9	5.9	4.9	5.6	6.5	4.2	3.4	5.3	3.4	7.8
U	1.3	3.2	1.5	2.0	1.3	2.7	1.0	1.2	1.7	1.7	2.1
Nb	5.7	13.1	5.9	4.8	7.6	9.5	5.0	4.4	5.8	4.3	11.1
Ta	4.4	8.5	4.3	4.2	0.5	0.7	0.4	0.4	0.7	0.5	0.7
La	18.7	39.1	18.0	14.0	19.3	25.2	12.3	11.9	15.3	12.5	27.6
Ce	37.9	49.0	36.8	29.0	38.7	52.0	25.1	28.0	35.0	30.0	56.6
Pb	5.3	12.9	4.3	4.5	4.2	3.9	2.8	4.0	5.8	6.5	4.7
Pr	4.4	9.3	4.3	3.4	4.5	5.9	3.0	2.9	3.6	3.0	6.6
Mo	0.7	1.0	0.6	0.7	0.7	1.1	0.5	1.0	1.4	1.9	0.5
Sr	202.1	90.7	72.3	173.7	113.1	172.5	105.0	90.2	92.0	75.6	169.4
P	420.2	609.4	352.9	389.7	222.6	281.5	157.1	154.9	183.3	157.1	333.9
Nd	17.3	35.1	16.8	13.5	17.4	22.8	11.7	11.4	13.8	11.8	25.1
Sm	3.9	6.8	3.5	3.1	3.6	4.7	2.7	2.6	3.0	2.8	5.2
Zr	91.3	168.8	85.5	81.3	90.6	129.3	66.2	67.1	80.0	65.6	137.7
Hf	3.1	5.3	2.8	2.5	2.5	3.6	1.9	1.9	2.3	1.9	3.8
Eu	1.3	1.3	0.9	1.1	1.0	1.1	0.7	0.7	0.8	0.7	1.1
Gd	4.6	6.5	3.8	3.6	4.0	5.4	3.3	3.4	3.7	3.5	5.3
Tb	0.9	1.1	0.7	0.7	0.7	0.8	0.6	0.6	0.6	0.6	0.9
Dy	5.9	6.8	4.5	5.1	4.3	5.2	3.8	3.8	3.9	4.0	5.4
Y	30.4	34.4	23.2	29.7	26.7	28.6	24.3	21.0	21.5	22.3	34.0
Ho	1.3	1.4	1.0	1.1	0.9	1.1	0.8	0.8	0.8	0.9	1.1
Er	3.8	4.1	2.9	3.3	2.7	3.2	2.5	2.4	2.5	2.6	3.4
Yb	3.8	3.9	2.7	3.2	2.7	3.3	2.6	2.6	2.5	2.7	3.4
Lu	0.6	0.6	0.4	0.5	0.4	0.5	0.4	0.4	0.4	0.4	0.5

Table S3. Sm/Nd isotopic analysis.

Sample Name	[Nd]	[Sm]	147Sm/144Nd	143Nd/144Nd	error	eNd(0)	eNd(t)	eNd(t) err	Tdm
TI10-012	26.07	5.25	0.1218	0.511710	0.000008	-18.1	-11.3	0.08	2.38
TI10-023	22.85	4.72	0.1249	0.511751	0.000006	-17.3	-10.8	0.06	2.40
TI10-030	28.91	5.74	0.1201	0.511724	0.000017	-17.8	-10.9	0.17	2.31
TI10-013	25.27	5.16	0.1234	0.511718	0.000010	-17.9	-11.3	0.10	2.41
TI11-016	28.74	5.90	0.1241	0.511692	0.000006	-18.5	-11.9	0.06	2.47
TI11-034	27.86	5.80	0.1259	0.511685	0.000033	-18.6	-12.2	0.33	2.53
TI11-005	21.50	4.50	0.1266	0.511766	0.000013	-17.0	-10.6	0.13	2.41
TI11-018	29.61	5.94	0.1212	0.511711	0.000008	-18.1	-11.2	0.08	2.36
TI11-018 Duplicate	33.42	6.77	0.1225	0.511716	0.000017	-18.0	-11.3	0.17	2.39
TI11-041	14.00	3.35	0.1445	0.511857	0.000008	-15.2	-10.5	0.08	2.84
TI11-003	20.84	4.58	0.1329	0.511778	0.000019	-16.8	-11.0	0.19	2.58
TI11-002	22.90	4.83	0.1274	0.511770	0.000008	-16.9	-10.6	0.08	2.43
TI11-010	25.11	5.22	0.1257	0.511722	0.000014	-17.9	-11.4	0.14	2.47
TI11-014	20.20	4.30	0.1287	0.511775	0.000005	-16.8	-10.7	0.05	2.46
TI11-038	18.01	3.84	0.1289	0.511768	0.000006	-17.0	-10.8	0.06	2.48
TI11-009	23.00	4.68	0.1231	0.511735	0.000003	-17.6	-10.9	0.03	2.37
TI11-008	29.37	5.96	0.1226	0.511701	0.000004	-18.3	-11.6	0.04	2.42
TI11-007	16.37	3.82	0.1411	0.511893	0.000006	-14.5	-9.5	0.06	2.63
TI10-025	25.59	5.30	0.1251	0.511775	0.000004	-16.8	-10.3	0.04	2.36
TI10-026	28.62	5.73	0.1210	0.511754	0.000008	-17.2	-10.4	0.08	2.29
TI11-013	10.78	2.65	0.1488	0.512032	0.000005	-11.8	-7.5	0.05	2.62
TI11-037	34.62	6.81	0.1189	0.511688	0.000007	-18.5	-11.5	0.07	2.34
TI11-017	15.76	3.53	0.1353	0.511834	0.000004	-15.7	-10.1	0.04	2.55
TI11-006	23.31	4.73	0.1225	0.511742	0.000004	-17.5	-10.7	0.04	2.35
TI10-011	43.45	8.74	0.1216	0.511669	0.000002	-18.9	-12.1	0.02	2.44